Advanced Steel Construction – Vol. 19 No. 3 (2023) 273–292
DOI:10.18057/IJASC.2023.19.3.8

RESEARCH ON SEISMIC BEHAVIOR OF L-SHAPED CONCRETE-FILLED STEEL TUBES COLUMN FRAME-BUCKLING RESTRAINED STEEL PLATE SHEAR WALLS

Amer Mohammed [1], Zhi-Hua Chen [1, 2], Yan-Sheng Du [1, *], W. A. H. Mashrah [3], Yu-Tong Zhang [1] and Mu-Wang Wei [4]

[1] *School of Civil Engineering, Tianjin University, Tianjin, 300072, China*
[2] *State Key Laboratory of Hydraulic Engineering Simulation and Safety, Tianjin 300072, China*
[3] *Dali Construction Group Co., Ltd, Hangzhou 310000, China*
[4] *School of Civil Engineering and Architecture, Wuyi University, Wuyishan, Fujian Province, China*
** (Corresponding author: E-mail: duys@tju.edu.cn)*

ABSTRACT

Frame buckling restrained steel plate shear walls (BRSPSWs) have been widely used in high-rise residential buildings. L-shaped concrete-filled steel tube (CFT) columns were used in the frame in this research to investigate the impact of the frame members type in the BRSPSWs system. A nonlinear finite element model (NFEM) was generated to examine the seismic performance of BRSPSWs with various types of connections to the frame elements. The NFEM results were compared to test results to make them more reliable, and the comparison showed that the NFEM can predict the seismic behavior of BRSPSWs. Then based on the validated NFEM results, several parameters were analyzed in parametric studies to assess their impact on the performance of BRSPSWs, including leg's length, column's width-to-thickness, axial compression ratio, and height-to-thickness of the steel plate, concrete panel's thickness, and bolt arrangement. The effect of these parameters on lateral resistance and yield stiffness was reported and discussed. A theoretical model has also been proposed based on modified plate-frame interaction (MPFI) to calculate the yield lateral resistance of BRSPSWs. The outcomes of MPFI were validated through testing and NFEM findings, and the comparison revealed reasonable concurrence.

ARTICLE HISTORY

Received: 18 October 2022
Revised: 17 April 2023
Accepted: 10 May 2023

KEYWORDS

Buckling restrained steel plate shear walls;
L-shaped CFT columns;
Nonlinear finite elements model;
Seismic performance;
Connection forms;
Modified plate-frame interaction

1. Introduction

Steel-plate-shear-walls (SPSWs) structures have been greatly utilized in high-rise buildings to resist earthquakes and wind loads [1-6]. A few decades ago, different types of SPSWs were proposed and studied, and it was found that the form of connecting the frame member to steel plates have a considerable impact on the overall behavior of SPSWs.

Astaneh et al. [7, 8] suggested and examined the effectiveness of SPSWs, consisting of precast concrete panels containing thin steel plates joined by the shear bolt (see Fig.1). Additionally, the objective of utilizing concrete panels is to prevent steel plates' buckling thereby improving the overall structure's lateral stability and energy absorption capacity. However, when these panels touch the boundary frame, the edges of the concrete panels often become deformed due to the force exerted on them. Consequently, the constraining effect of the concrete panels on the thin steel plate is diminished. Accordingly. A novel SPSWs system proposed by Astaneh et al. [9], making a gap between the boundary elements and concrete panels. Similarly, the lateral resistance will be impacted marginally by concrete panels, improving the steel plate's buckling resistance. After that, scholars concluded that the concrete panels get partly deformed causing by shear bolts and nuts, leading to shear deformation. According to the Astaneh's model, an improved buckling-restrained steel plate shear wall was suggested by Guo et al [10], which placed oval holes on the concrete panels to prevent huge damage to panels around shear connectors. The main function of sandwiching the inner steel plate by concrete is to constrain the local buckling and out-plan deformation. According to the research findings, the BRSPSWs have exhibited remarkable lateral resistance and seismic performance [10].

Conversely, research indicates that the connections linking frame elements and the stiffness of the framework significantly impacted the seismic performance of SPSW. Thus, academics have put forth various types of connections as potential solution such as low yield light-gauge and point SPSW [11, 12], perforated SPSW panels [13], partially connected to beam only SPSW [14], steel plate slits SPSW [15], buckling-restrained steel SPSW with inclined-slots [16] bound-columns with buckling-restrained SPSW [17], and partially connected bucking SPSW [18] to overcome steel plate's local buckling and to minimize the stiffness of vertical boundary elements (VBEs). In contrast, the manufacture and construction of these linkages involve intricate processes, which lead to the use of suboptimal materials and reduced economic efficiency. Furthermore, a group of scholars has proposed a new type of partial connection inner BRSPSW as a solution to generate a robust system capable of withstanding lateral forces while requiring low stiffness requirements for VBEs [19-22].

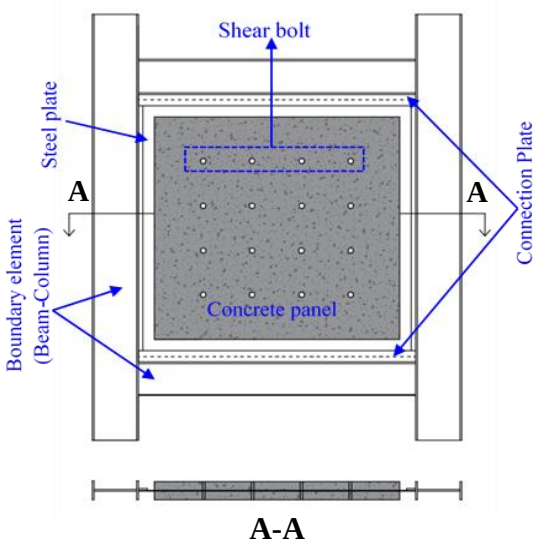

Fig. 1 Strip model of steel plate shear walls [2]

The seismic performance of buckling-restrained SPSWs with four side connections was well examined [23-27]. Buckling-restrained SPSWs showed better lateral stiffness, lateral resistance, and energy consumption than unconstrained SPSW. The transferred force from boundary columns to SPSWs in four-sided buckling-restrained SPSWs may cause early deformation on columns [26]. Diagonal local buckling and fracture at the corner steel plates always happened. Also, the size of buckling-restrained SPSWs should be a little large to build the four-side connections steel plate to connect it with the boundary frames [25, 26]. Buckling-restrained SPSWs with two-side connections were designed and studied to exceed the premature deformation of columns. It was found that the buckling-restrained SPSW with two-side connections has an excellent deformation capacity. Still, the lateral resistance and energy consumption were less than BRSPSW with four-side connections [14, 24, 28, 29].

Furthermore, several studies were carried out in SPSW using various VBEs such as H-section and CFT columns [18, 22, 30, 31]. Chen et al. [32-34] suggested and studied axial behavior and presented a superposition approach for determining ultimate capacity [35-37]. To boost the application of CFT columns, Zhou et al [38]. carried out a test and FE modeling study on a special-shaped CFT column frame shear wall and inspected the effect of the

compression load ratio on the stiffness of the frame. The findings presented that the frame has good seismic performance with lateral resistance, ductility.

This paper firstly conducted an experimental program on BRSPSWs under lateral cyclic loads. Then three-dimensional NFEM was established using a commercial finite element application ABAQUS CAE to simulate the seismic performance of BRSPSWs. Based on validated NFEM, parametric analyses were generated to evaluate the impact of critical aspects, including leg's length, width-to-thickness of column, compression load, the steel plate's height-to-thickness of, thickness of the concrete panel, and bolt arrangements. All parameters were discussed based on lateral resistance and stiffness. Finally, a modified calculation approach has been suggested for calculating the lateral resistance at yield point, and it was validated against the test and parametric models' results.

2. Test program

An experimental program [22] with three specimens was included in this research paper to prove the accuracy of numerical simulation on the seismic performance of frame-buckling restrained steel plate shear walls (BRSPSWs).

2.1. Specimens' design

Three of 1/2 scale specimens with one bay and two floors were designed to study the seismic behavior of BRSPSWs with various types of connections between boundary members, as illustrated in Fig.2. The methodology and geometric configuration were obtained from an engineering endeavor in China. H-section beam and L-shaped CFT columns manufactured horizontal and vertical boundary elements, respectively. To create the L-shaped CFT columns, three square steel tubes were linked with two vertical plates by welding connection, as shown in Fig.3. Additionally, to link the columns and beams, Vertical stiffeners were employed to connect the L-shaped CFT column to the beam, as depicted in Fig. 4.

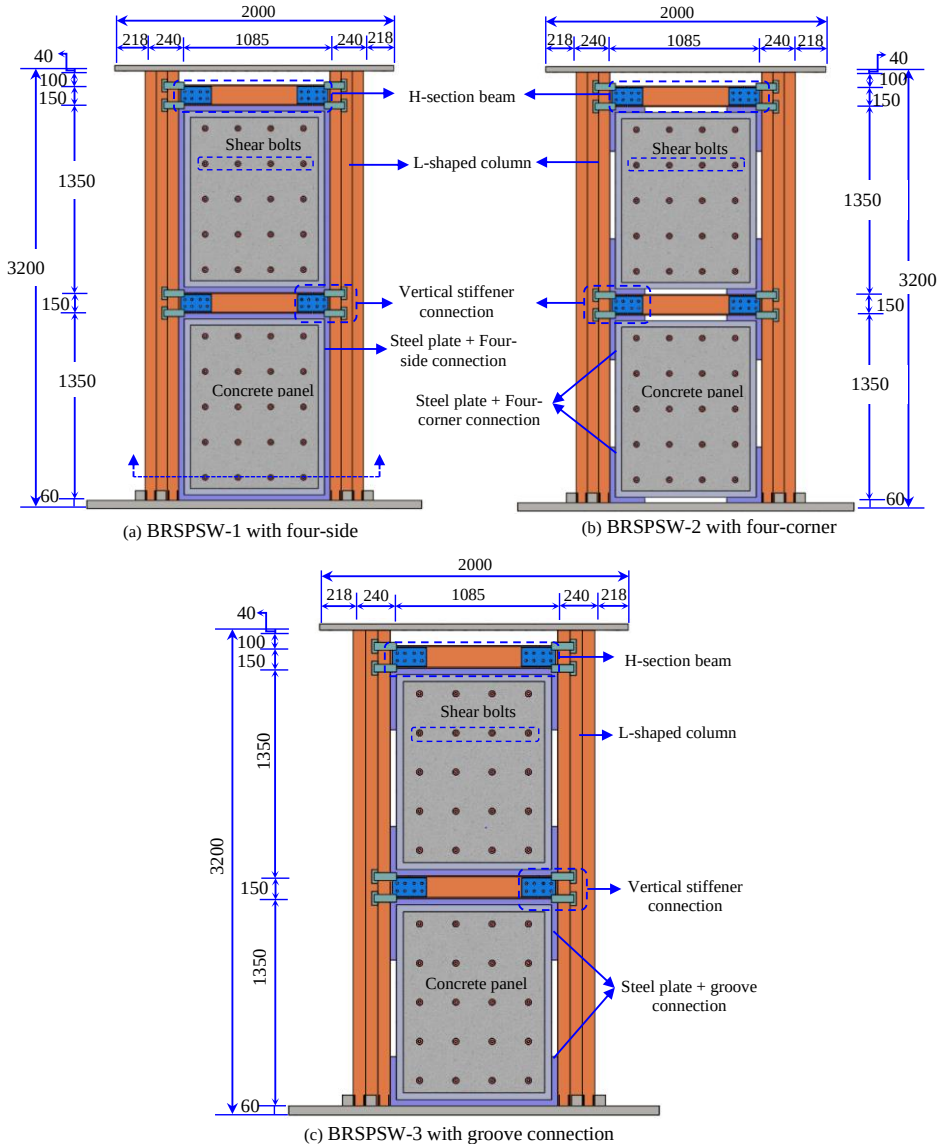

(a) BRSPSW-1 with four-side (b) BRSPSW-2 with four-corner

(c) BRSPSW-3 with groove connection

Fig. 2 Elevation view of specimens

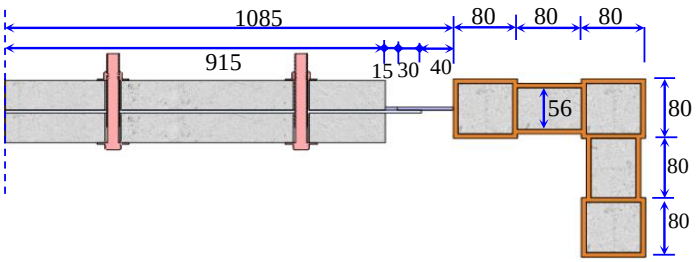

Fig. 3 Top view of column-shear wall connection

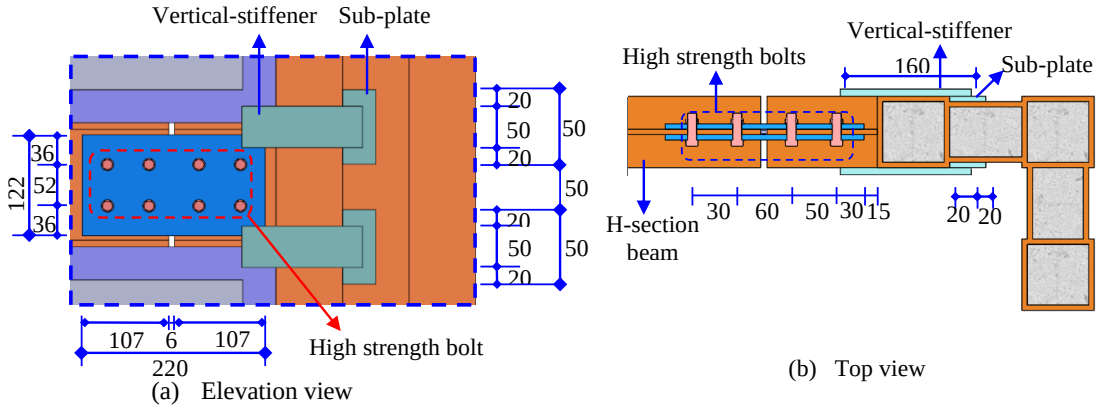

Fig. 4 Beam-column connection

Three kinds of connections have been utilized to link the steel plates to the frame members, namely four-side, four-corner and groove connections corresponding to the subsequent specimens, BRSPSW-1, BRSPSW-2 and BRSPSW-3. In greater details, the four-side indicates that the inner steel plate was completely linked with the frame members Fig. 5(a), since the four-corner was partly linked by 320mm and 250mm to the columns and beams, as seen in Fig. 5(b). Likewise, the beams were entirely connected to the inner steel plate while partially with columns (see Fig. 5(c)). The two concrete panels sandwiched steel plate using high-strength bolts to constrain its early buckling. Besides, the concrete panels were two-way reinforced with HPB235 by a one sheet.

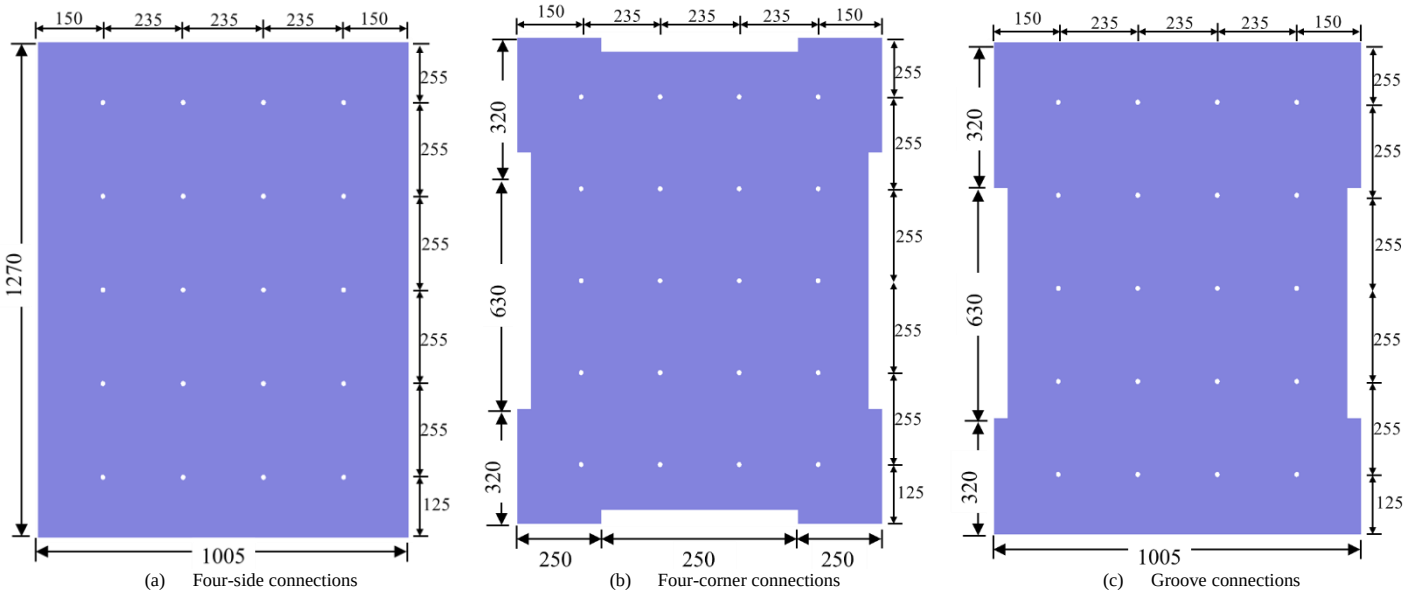

Fig. 5 Details of buckling steel plates

2.2. Material properties

All steel tubes, H-section beams, and steel plates were manufactured using Q235 steel. A tensile coupon test was conducted on different material types and thicknesses to determine the mechanical properties based on the Chinese guidelines GB/T 228.1–2010 [39], as seen in Fig.5(a). Engineering stress-strain relationships acquired from the steel material testing are illustrated in Fig. 5(b). The outcomes of each coupon's mean yield and ultimate strength, the elasticity of modulus, and fracture of strain are listed in Table 1. Notable, thickness has an impact effect on strength and stiffness.

Concrete panels and infill are both constructed using normal-grade C40 concrete. Six cubes **100 × 100 × 100 mm** concrete cube was designed and tested in accordance with the GB/T50081-2019 [40] guidelines to determine the mechanical properties. The mean values of elasticity of modulus and compressive strength were 236 GPa and 41.59 MPa.

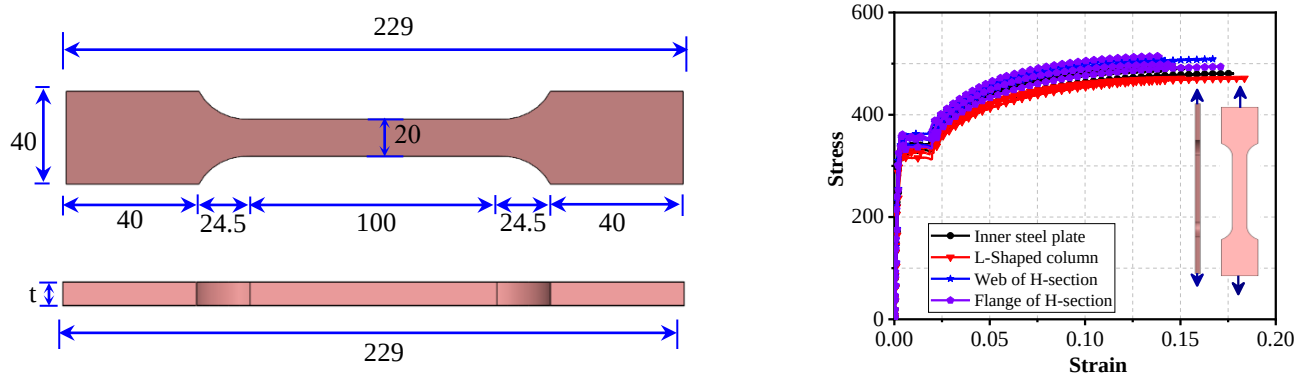

Fig. 6 Steel material test

Table 1
Test results of steel material properties

Elements	Thickness (mm)	f_y (MPa)	f_u (MPa)	E (MPa)	f_y/f_u	ε_f
Steel tubes for L-Shaped column	6	306	469	168	0.65	0.141
Web of H-section	6	338	502	176	0.67	0.169
Flange of H-section	8	339	508	176	0.67	0.168
Inner steel plates	4	327	488	172	0.67	0.165

Note: f_y yield strength, f_u refers ultimate strength, E is elasticity of modulus, ε_f is the fracture strain

2.3. Test setup and loading protocol

The specimens were positioned on the rigid floor and linked to it by high-strength bolts to approach fixed ends, as illustrated in Fig. 7. The specimens underwent lateral cyclic loading using a 300-ton bi-directional hydraulic actuator that was connected to the loading beam on the top plate. Besides, to consider the impact of the slab restraints in the horizontal orientation of the actual buildings, steel tubes were put at the top of each story.

Fig. 8. illustrates the recorded horizontal loading data for BRSPSWs, which was obtained by applying the Chinese standard JGJ 101-2015 [41]. The loading progression was classified into the force-control phase and displacement-control phase. During the load-control phase, one cycle with a 20 % interval from the yield load ($\boldsymbol{P_y}$) was adopted to apply the loading-control phase. Subsequently, the displacement-control phase took over from the load-control phase, where the displacement increments for each level were determined by the yield displacement (Δ_y), and three uniform cycles were executed for each level, as seen in Fig.8. Finally, the loading procedure was interrupted in two scenarios; firstly, when the lateral resistance had declined to eight five percent after reaching the maximum resistance, and secondly, once the samples had undergone complete damage.

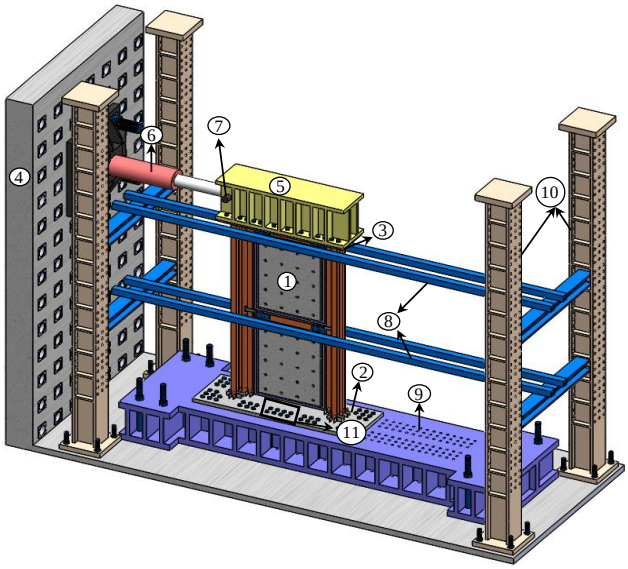

1. Specimen; 2. Bottom plate; 3. Top plate; 4. Reaction wall; 5. Loading beam; 6. Hydraulic actuator; 7. Hinged joint; 8. Square steel tubes; 9. Foundation; 10. Reaction frame; 11. High strength bolts

Fig. 7 Test setup of BRSPSWs under lateral cyclic loads

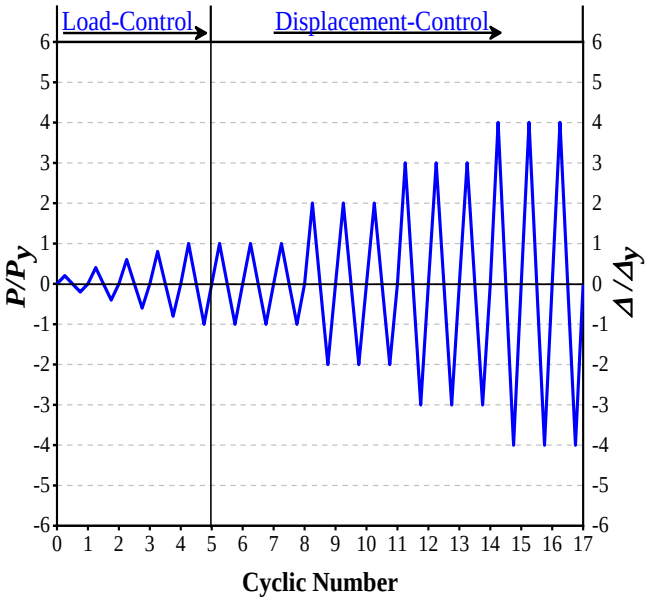

Fig. 8 Time-history of loading BRSPSW

3. Finite element model

As mentioned above, the main target of the tests was to validate the accurateness of the numerical outcomes. Even though the test program revealed valuable investigation, the results are inadequate for further analysis of BRSPSWs. Thus, generating nonlinear finite element models (NFEM) is mandatory to deeply understand the performance of BRSPSWs with critical parameters obviating conducting a new additional testing program [42].

3.1. General

ABAQUS explicit/solver was adopted to build more FE models. Additionally, to obtain high accuracy in the explicit/solver, geometrical, material nonlinearities, meshing convergence, complicated contact pairs, loading rate, and boundary conditions were considered during simulation.

3.2. Material models

All steel components were modeled using nonlinear isotropic/kinematic hardening. Q235 steel components was undergoing cyclic loading and unloading according to a five-stage uniaxial stress-strain model, as shown in Fig. 9. and Eq (1). The mechanical properties acquired from the material test were inserted during modeling. In addition, shear and ductile damage were employed to replicate steel materials' tearing and fracture behavior in modeling [43].

$$\sigma_s = \begin{cases} E_s\varepsilon_s & ,\varepsilon_s \le \varepsilon_e \\ -A\varepsilon_s^2 + B\varepsilon_s + C & ,\varepsilon_e \le \varepsilon_s \le \varepsilon_{e1} \\ f_y & ,\varepsilon_{e1} \le \varepsilon_s \le \varepsilon_{e2} \\ f_y[1+0.6(\varepsilon_s-\varepsilon_{e2})/(\varepsilon_{e3}-\varepsilon_{e2})] & ,\varepsilon_{e2} \le \varepsilon_s \le \varepsilon_{e3} \\ 1.6f_y & ,\varepsilon_s \le \varepsilon_{e3} \end{cases} \quad (1)$$

where E_s is steel elastic modulus, σ_s and ε_s denote the stress and strain of steel respectively; f_y indicates the yield strength of steel; $\varepsilon_e, \varepsilon_{e1}$, and ε_{e2} represents the medium strain; ε_{e3} is the ultimate strain; A, B and C are constant. All strain values and constants can be calculated as follows.

$$\varepsilon_e = 0.8\frac{f_y}{E_s};\quad \varepsilon_{e1} = 1.5\varepsilon_e;\quad \varepsilon_{e2} = 10\varepsilon_{e1};\quad \varepsilon_{e3} = 100\varepsilon_{e1} \quad (2)$$

$$A = 0.2\frac{f_y}{(\varepsilon_{e1}-\varepsilon)^2};\quad B = 2A\varepsilon_{e1};\quad C = 0.8f_y + A\varepsilon_e^2 - B\varepsilon_e \quad (3)$$

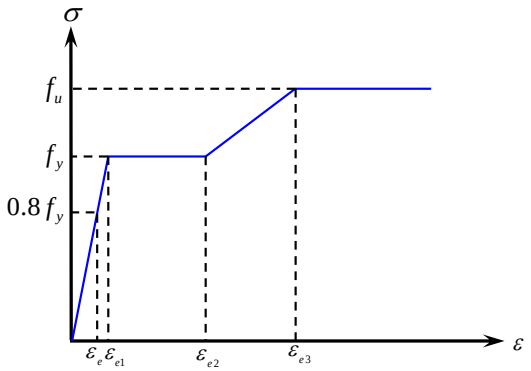

Fig. 9 Stress-strain model for steel materials

The concrete infill and panels were simulated using the concrete damage plasticity model. Two failure mechanisms were assumed to accurately model infill concrete and precast concrete's behavior, which are compressive and tensile behavior. On the other hand, Han's stress-strain relationship was adopted to categorize the plastic behavior of the concrete [44]. The following mathematical equations can express the stress-strain relationship.
For concrete compressive behavior,

$$y=\begin{cases}2x-x^2 & ,x\le 1\\ \dfrac{x}{\beta_0(x-1)^{1.6+1.5/x}+x} & ,x>1\end{cases}\qquad x=\frac{\varepsilon_c}{\varepsilon_{c0}};y=\frac{\sigma_c}{\sigma_{c0}} \tag{4}$$

In which

$$\sigma_{c0}=\left[1+(-0.0135\xi+0.1\xi)\left(\frac{24}{f_c^{'}}\right)^{0.45}\right]f_c^{'} \tag{6}$$

$$\varepsilon_{c0}=[(1300+760(\frac{f_c^{'}}{24}-1)]\xi^{0.2}\times 10^6 \tag{7}$$

$$\varepsilon_0=(1300+12.5f_c^{'})\times 10^6 \tag{8}$$

$$\beta_0=\begin{cases}\dfrac{(f_c^{'})^{0.1}}{1.35\sqrt{1+\xi}} & ,\xi\le 3\\ \dfrac{(f_c^{'})^{0.1}}{1.35\sqrt{1+\xi}(\xi-2)^2} & ,\xi>3\end{cases} \tag{9}$$

$$\xi=\frac{A_s f_y}{A_c f_{ck}} \tag{10}$$

For concrete tensile behavior,

$$y=\begin{cases}1.2x-0.2x^6\\ \dfrac{x}{0.31\sigma_{t0}(x-1)^{1.7}+x}\end{cases} \tag{11}$$

In which

$$x=\frac{\varepsilon_t}{\varepsilon_{t0}};y=\frac{\sigma_t}{\sigma_{t0}} \tag{12}$$

$$\sigma_{t0}=0.26(1.25f_c^{'})^{2/3} \tag{13}$$

$$\varepsilon_{t0}=0.0000431\sigma_{t0} \tag{14}$$

where $\sigma_{c0},\varepsilon_{c0}$ are compressive stress and strain of concrete, respectively f_y and A_s denote the yield strength of steel tubes and cross-sectional area; f_{ck} and A_c indicate compressive strength of concrete and its cross-sectional area; $f_{ck}=0.67f_{cu}$ for normal concrete; $f_c^{'}$ and f_{cu} are cylinder and cube of concrete's compressive strength, the elastic modulus elasticity of concrete could be determined according to ACI-318 code as $E_c=4730\sqrt{f_c^{'}}$ [45]; Poisson's ratio $\nu=0.2$ for concrete. Additionally, $\varepsilon_{t0},\sigma_{t0}$ refer to the tensile strain and stress of concrete, respectively.

3.3. Elements and meshing convergence

Each deformable part's three-dimensional simulation was carried out using hex-structured mesh controls, including a linear brick with eight nodes, hourglass-shaped and reduced integration control element of type C3D8R. A sequence of meshing convergence was take into account during simulation to make an equilibrium between the accuracy of numerical modeling and computing efficiency. Figs. 10(a) and (b) present the assemble and meshing dimension of all elements of the structures.

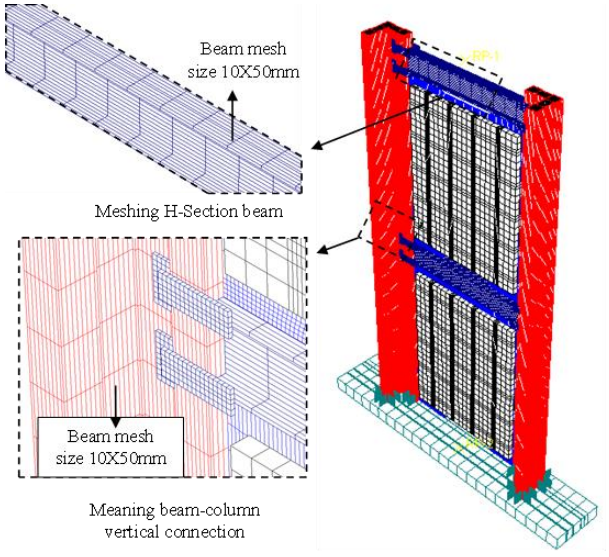

(a) Meshed element model

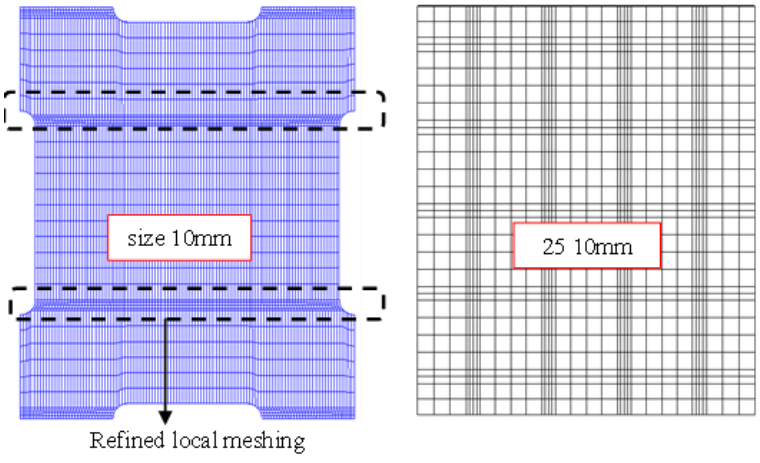

(b) Refined Meshing of inner steel plate and concrete panel

Fig. 10 Typical meshing of finite element model

3.4. Interactions and boundary conditions

All steel members were tied together to simulate welding performance, including lower boundary plate, frame elements, and steel plates. Due to the complex interaction among bolts, concrete panel, and steel plates, the concrete panels were tied to the steel plates at specific positions, as illustrated in Fig. 11. These specific positions chosen at the concrete panels and tied to the steel plates could simulate the bolt functions in the tested specimens regarding connecting the concrete panels to the steel plate (see Figs. 2-3). To establish how the concrete panels and steel components interact, a surface-to-surface

contact algorithm was utilized. A hard contact method was employed in the perpendicular direction, while a penalty friction model with a coefficient of 0.6 was implemented in the parallel directions [46, 47]. The slave and master surfaces were determined based on the relative hardness of the materials.

Fig. 11. demonstrates the simulation of loading and boundary conditions. The top surfaces of the columns were coupled to a reference loading point, and then the lateral load was applied as displacement loading. Four constrained beams with fixed ends were launched on both upper sides of each story to simulate square steel tubes for the tests, and these beams were restrained in both displacement and rotations. The test also restrained displacement and rotation for emulating fixed support. To account for initial defects and the buckling modal of steel plates during simulation, the first eigenmode was chosen as the buckling modal allocation.

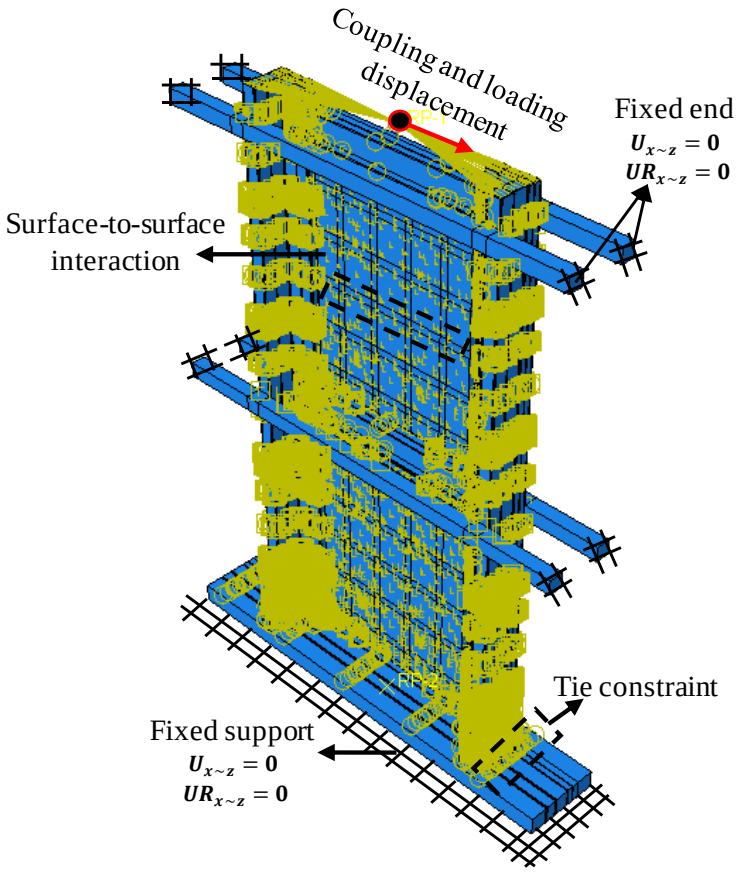

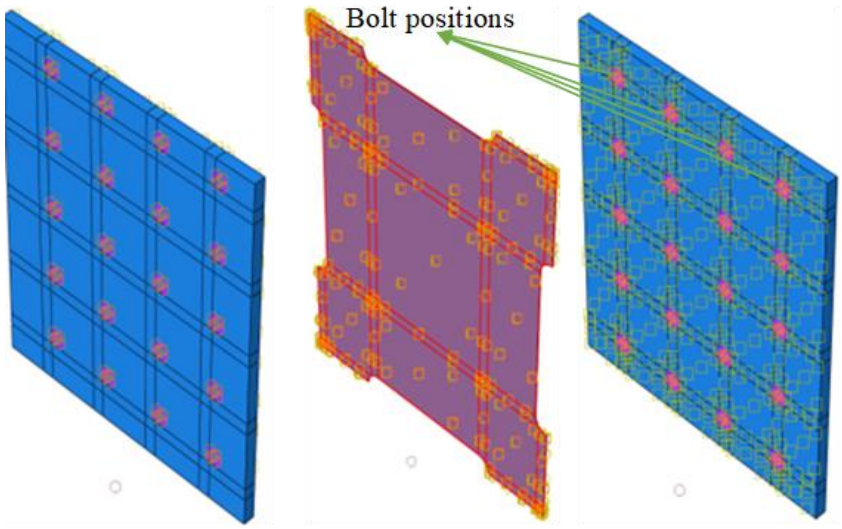

Fig. 11 Numerical simulation details in interactions and boundary conditions

3.5. Validations

3.5.1. Comparison of failure modes

Fig. 12. compares the FE simulation with an experimental program of deformation shapes and failure modes of BRSPSW-1, 2 and 3. It noticed that the FE simulations could accurately predict the failure patterns of BRSPSWs. Firstly, the manifestation of damage on BRSPSW-1 is assigned to the occurrence of concrete crackling at the intersection of the concrete panels, coupled with the fracturing and impairment of the column. Furthermore, it has been observed that the lateral resistance of BRSPSW-1 deteriorated sharply to less than 85%, and the lower section of the boundary columns in BRSPSW incurred extensive damage, primarily owing to the adverse fully connected of the steel plate to the frame members, as displayed in Fig. 12(a). Secondly, the BRSPSW-2 system effectively detected both inner steel plates' local buckling and concrete cracking at the corners of the panels owing to its distinct configuration of separating the inner steel plate and concrete panels, as seen in Fig. 12(b). Conversely, the boundary columns remained undamaged even though the effective connected area of the frame to steel plates between the

was reduced. Finally, Fig. 12(c). depicts the comparison of deformation shaped between FE-simulation and test phenomenon. BRSPSW-3 experienced multiple failures, including local buckling of the steel plate, cracking of concrete panels, and fractures and tears in both the frame members and inner steel plate. Subsequently, considering the high accuracy and adequacy of NFEM, elaborating parametric studies is suitable and recommended.

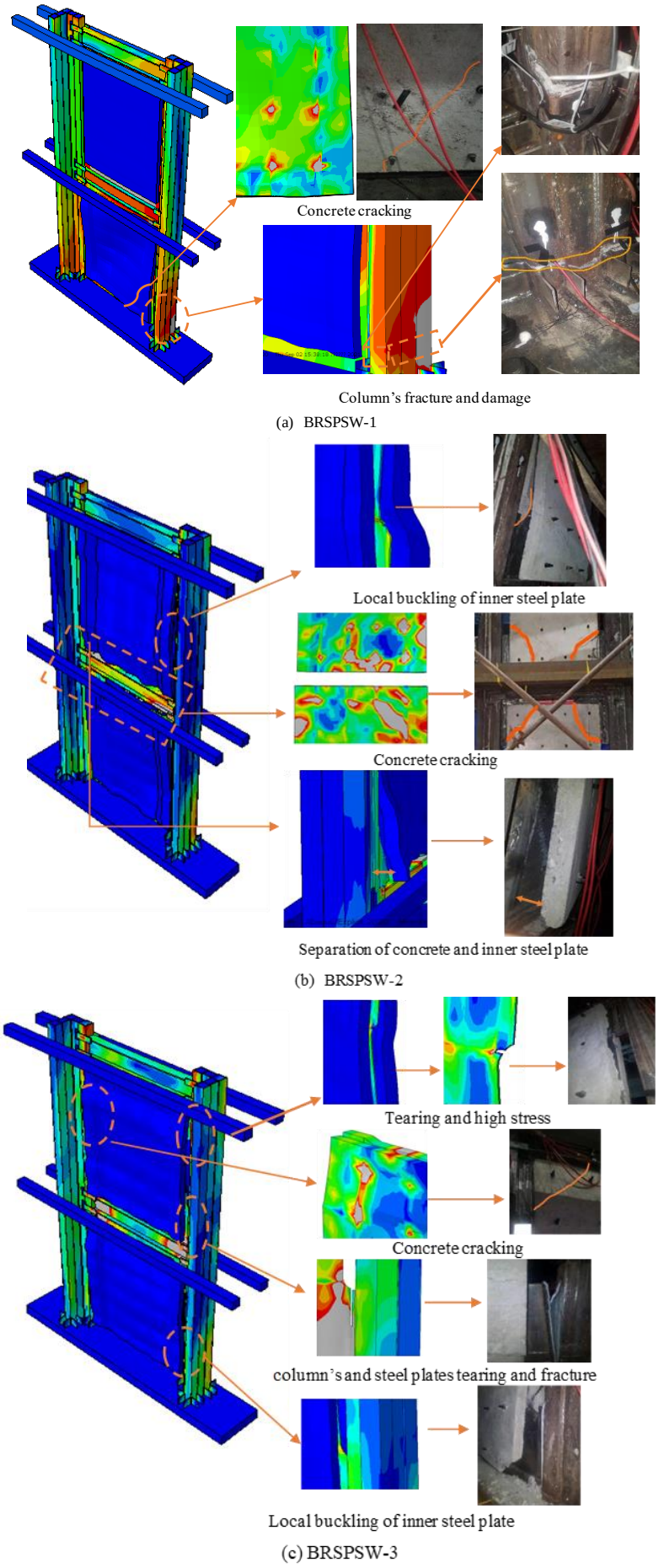

Fig. 12 Validation of failure modes between experiments and numerical simulations

3.5.2. Comparison of hysteretic and skeleton curves

Fig. 13(a-c). compares the experimental load versus displacement $(P\text{-}\Delta)$ curves with FE-simulation results. It shows that the FE simulations can precisely simulate the hysteresis and skeleton curves of BRSPSWs. The behavior of both hysteretic and skeleton curves remains the same for both test and FE modeling results. Besides, the pinching effect in the hysteretic curves was observed in both the test and FE models outcomes, and it shows that the pinch behavior is mainly affected by connection forms. In BRSPSW-3, the pinch behavior appeared clearer than others due to the steel plates' local buckling, while the BRSPSW-1 is the fullest among them, according to Fig. 13 and Table 2. A comparison was made between the test results and the corresponding FE predictions for yield, peak lateral resistance, and yield stiffness in both positive and negative directions. The mean value of test-to-FE simulations of yield and peak lateral resistance was (1.02 & 0.99) with standard deviations (0.05, 0.04). The average lateral yield stiffness is (0.97) with std.v (0.03). Consequently, FE simulation could predict the performance of BRSPSWs subjected to lateral cyclic load.

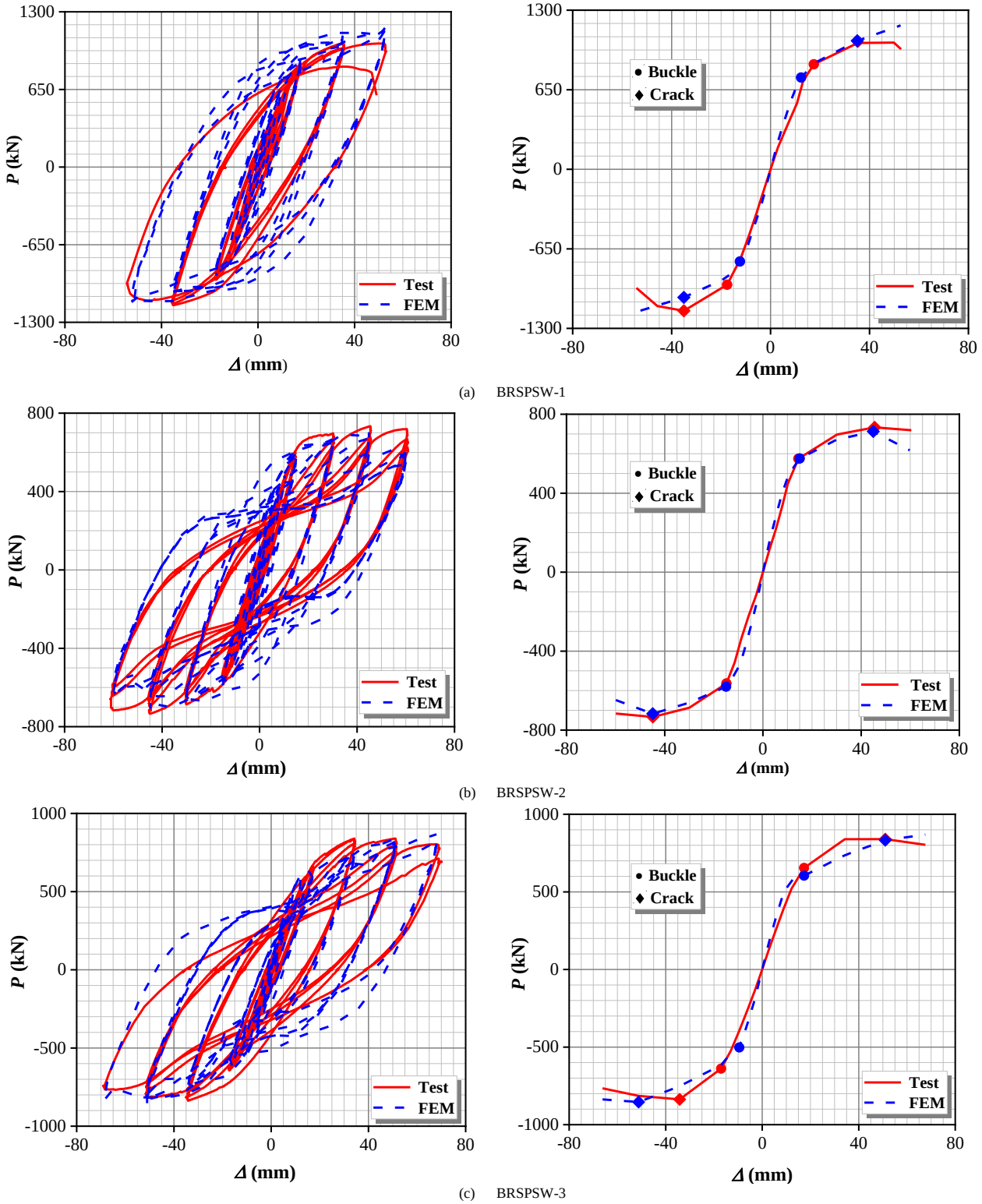

Fig. 13 Comparisons of load-displacement relationship of tests-to-FE-models

Table 2
Comparison test-to-prediction ratios for P_y, P_m and K_y

items	$P_{y,Test}$ (kN)	$P_{y,FE}$ (kN)	$\frac{P_{y,Test}}{P_{y,FE}}$	$P_{m,Test}$ (kN)	$P_{m,FE}$ (kN)	$\frac{P_{m,Test}}{P_{m,FE}}$	$K_{y,Test}$ $(\frac{kN}{mm})$	$K_{y,FE}$ $(\frac{kN}{mm})$	$\frac{K_{y,Test}}{K_{y,FE}}$

	+	878.00	922.00	0.95	1038.90	1176.30	0.88	43.25	46.33	0.93
BRSPSW-1	-	-956.10	-949.00	1.01	-1156.90	-1155.30	1.00	49.80	47.21	1.05
	Avg	**917.05**	**935.50**	**0.98**	**1097.90**	**1165.80**	**0.94**	**46.52**	**46.77**	**0.99**
	+	590.80	595.20	0.99	733.70	712.80	1.03	35.38	36.97	0.96
BRSPSW-2	-	-585.20	-595.50	0.98	-733.30	-717.10	1.02	32.69	34.62	0.94
	Avg	**588.01**	**595.35**	**0.99**	**733.50**	**714.95**	**1.03**	**34.03**	**35.80**	**0.95**
	+	694.40	620.50	1.12	840.00	869.40	0.97	36.17	31.34	1.15
BRSPSW-3	-	-670.10	-645.80	1.04	-873.20	-853.80	1.02	33.84	32.13	1.05
	Avg	**682.25**	**633.15**	**1.08**	**856.60**	**861.60**	**0.99**	**35.01**	**31.73**	**1.10**
Mean value				1.02			0.99			0.97
Std.v				0.05			0.04			0.03

Note: $P_{y,Test}$, $P_{y,FEM}$, $P_{m,Test}$, $P_{m,FEM}$, $K_{y,Test}$ and $K_{y,FEM}$ signify test value of yield, peak resistance, and yield stiffness gained from experiments and FE-modeling, respectively. The yield stiffness can be calculated as follows K_y P_y/Δ_y. The general yield moment method is adopted to calculate yield point, as seen in Fig. 14.

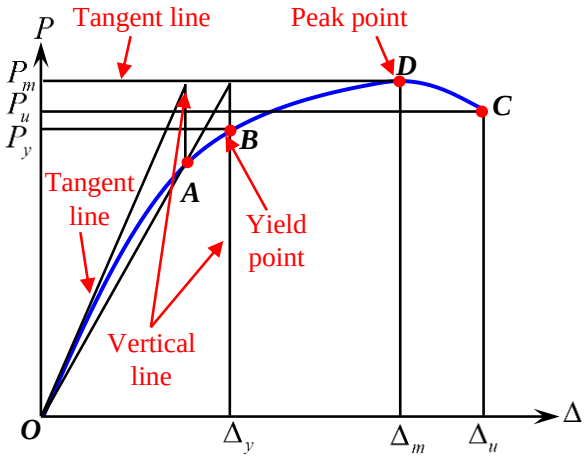

Fig. 14 Yield point determinations diagram

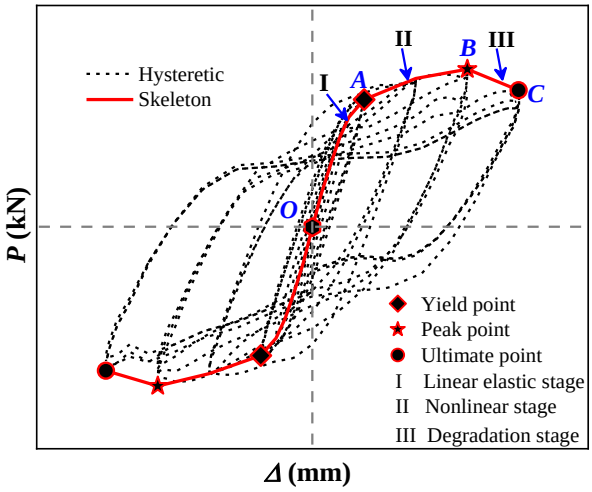

Fig. 15 General classification of hysteretic and skeleton curves

4. Numerical parametric studies on BRSPSW

4.1. General behavior

Fig. 15. plots P-Δ (hysteretic and skeleton) curves. From the test and FE-simulated results in (Fig. 13(a-c)), it can be observed that all P-Δ curve has three stages, including linear, nonlinear and degradation stages. As seen in Fig. 15, at linear stage (I), (i.e., *OA)*, the cyclic load of the BRSPSWs increase linearly with the increasing lateral displacement. At the end of the linear stage, the yield point of BRSPSWs was achieved. Nonlinear with pinch behavior is observed during the nonlinear stage (II), (i.e., curve *AB* in Fig. 15.) owing to of inner steel plates' local buckling resistance, and the peak point was achieved at the end of this stage. After the samples reached their peak points, the degradation stage (II) started. When the lateral resistance reached 85% of peak lateral resistance, the models achieved their ultimate points (i.e., *BC* in Fig. 15.)

4.2. Failure modes

Generally, high stress on bolts' positions was appeared on the concrete panels, indicating cracking on the concrete panels stared from bolts holes due to buckling on inner steel plates, as shown in Fig. 16(a). With increasing the lateral displacement, the local buckling of steel plates started from their edges and developed with appearing diagonally. As seen in Fig. 16(b), it appeared diagonally in the nonlinear phase. after that, due to the large local buckling of steel plate, concrete separation and out-plane deformation was obvious, indicating less buckling resistance by concrete panels (see Fig.16 (a&b)). In the degradation stage, the concrete panels were severely damaged, and the inner steel plate was torn because of their instability to resist the overall buckling (see Fig. 16(b)). Finally, the column was buckled at the bottom, as shown in Fig.16(c).

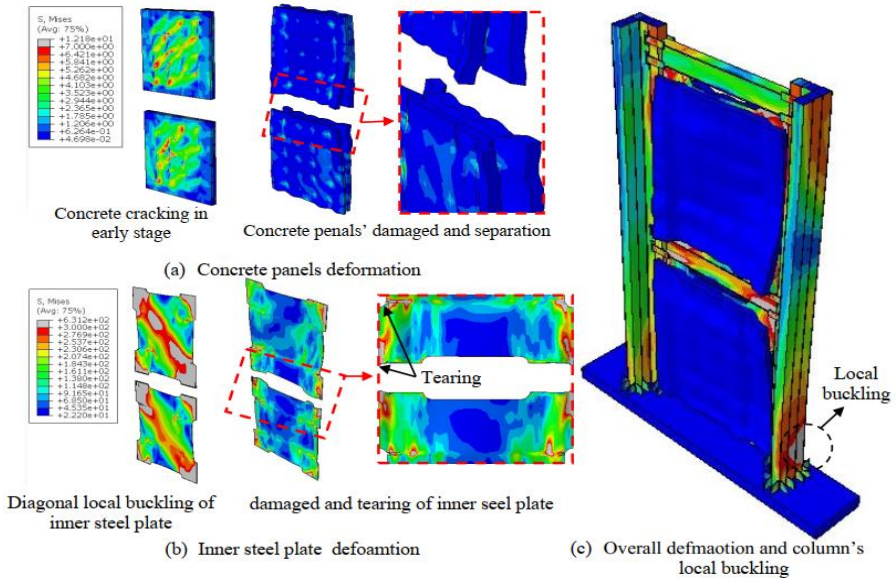

Fig. 16 Overall FE-failure modes of BRSPSW

4.3. Details of cases in the parametric studies

After verifying the numerical results via comparing them with experimental results of BRSPSWs under cyclic loading, numerical parametric investigations were executed to explore the impact of crucial factors, including leg's length (L_p), columns' width-to-thickness (D/t), axial compression ratio (n_d), the inner steel plates' height-to-thickness ratio, thickness of the concrete panels (t_c), and bolt arrangements ($B(RxC)$), as listed in Table 3. Besides, BRSPSW-2 was chosen as a reference to study all these parameters. The yield and peak lateral resistance (P_y & P_m) and lateral yield stiffness (K_y) was used to analyze the behavior of BRSPSWs. The lateral yield stiffness can be determined as the following equation.

$$K_y = \frac{P_y}{\Delta_y} \tag{15}$$

in which K_y is the ratio of yield lateral resistance P_y to its corresponding yield displacement Δ_y .

Table 3
Details of different cases of parametric studies

Samples	Models' ID	L_p (mm)	D/t (%)	n_d (%)	t_s (mm)	t_c (mm)	$B(RxC)$ #
Impact of leg's length	L_P=150	**150**	13.33	0 %	4	40	B(4x5)
	L_P=200	**200**	13.33	0 %	4	40	B(4x5)
	L_P=250	**250**	13.33	0 %	4	40	B(4x5)
	L_P=300	**300**	13.33	0 %	4	40	B(4x5)
	L_P=350	**350**	13.33	0 %	4	40	B(4x5)
	L_P=400	**400**	13.33	0 %	4	40	B(4x5)
Impact of column's width-to-thickness	D/t=20	250	**20.0**	0 %	4	40	B(4x5)
	D/t=16	250	**16.0**	0 %	4	40	B(4x5)
	D/t=13.3	250	**13.3**	0 %	4	40	B(4x5)
	D/t=11.4	250	**11.4**	0 %	4	40	B(4x5)
	D/t=10	250	**10.0**	0 %	4	40	B(4x5)
Impact of axial compression ratio	n_d=0 %	250	13.33	**0 %**	4	40	B(4x5)
	n_d=25 %	250	13.33	**25 %**	4	40	B(4x5)
	n_d=50 %	250	13.33	**50 %**	4	40	B(4x5)
	n_d=75 %	250	13.33	**75 %**	4	40	B(4x5)
	n_d=100 %	250	13.33	**100 %**	4	40	B(4x5)
Impact of Height-to-thickness ratio	t_s=2	250	13.33	0 %	**2**	40	B(4x5)
	t_s=3	250	13.33	0 %	**3**	40	B(4x5)
	t_s=4	250	13.33	0 %	**4**	40	B(4x5)
	t_s=5	250	13.33	0 %	**5**	40	B(4x5)
	t_s=6	250	13.33	0 %	**6**	40	B(4x5)
Impact of concrete panel's thickness	t_c=20	250	13.33	0 %	4	**20**	B(4x5)
	t_c=30	250	13.33	0 %	4	**30**	B(4x5)
	t_c=40	250	13.33	0 %	4	**40**	B(4x5)
	t_c=50	250	13.33	0 %	4	**50**	B(4x5)
	t_c=60	250	13.33	0 %	4	**60**	B(4x5)
Impact of bolt arrangements	B(4x5)	250	13.33	0 %	4	40	**B(4x5)**
	B(4x3)	250	13.33	0 %	4	40	**B(4x3)**
	B(4x2)	250	13.33	0 %	4	40	**B(4x2)**
	B(2x3)	250	13.33	0 %	4	40	**B(2x3)**
	B(2x2)	250	13.33	0 %	4	40	**B(2x2)**

Note: L_p denotes the leg's length of steel plate connection; D/t denotes column's width-to-thickness; n_d denotes the axial compression ratio; t_s denotes the thickness of the steel plate; t_c denotes the concrete panel's thickness; *B(RxC)* denotes the number of bolts arrangements

4.3.1. Influence of leg's length of steel plate

The behavior of BRSPSWs under cyclic load is greatly affected by the connection form of the inner steel plate with the boundary elements [18]. Therefore, the FE-model of the BRSPSW-2 was selected as a reference model in which leg's length $L_p = 250mm$ was adopted (see Fig. 5(b)). Then other FE-models were simulated with different leg's length values (*150mm,200mm,300mm,350mm and 400mm*). The comparison load-displacement curves (hysteretic and skeleton) are represented in Fig. 17 (a-b). It can be noticed that the leg's length did not greatly influence initial stiffness and ductility. Fig. 17(c) plots the yield, peak lateral resistance, and lateral yield stiffness, showing that the lateral resistance increased with the leg's length. However, yield and peak lateral resistance slightly increased when the leg's length was 150, 200, and 250 Fig. 17(c). Then they dramatically increased when the legs were 300mm,350mm, and 350mm. Besides, the lateral yield stiffness showed a slight growth when leg's length was less than 250mm, but when the leg's length was more than 300mm, the stiffness suddenly jumped.

Then it almost remained stable. Consequently, it can be concluded that the leg's length greatly influenced the yield and peak lateral resistance. Still, it is not recommended when the leg's length is less than 250mm due to its negative effect on ductility.

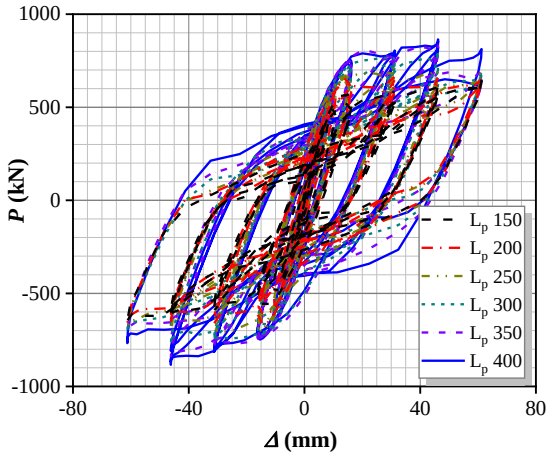

(a) Comparison of hysteretic curves

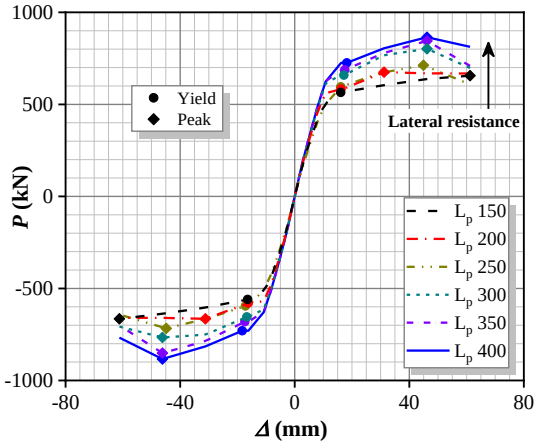

(b) Comparison of skeleton curves

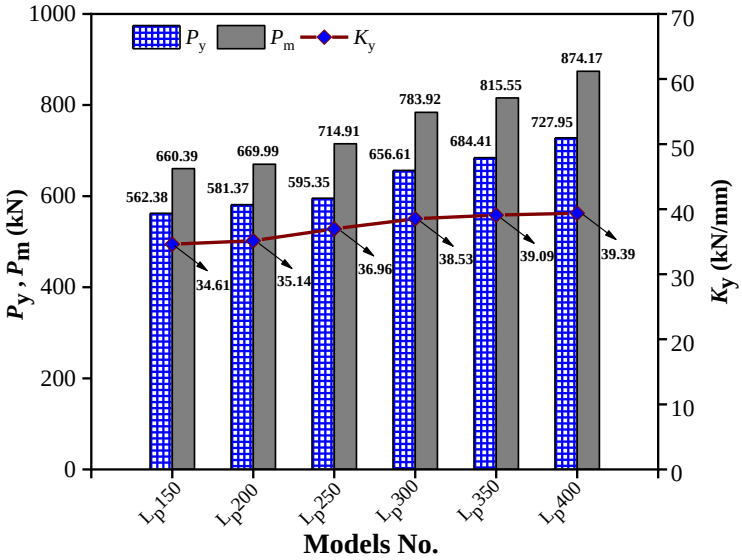

Fig. 17 Impact of length of leg connected to steel plate on lateral resistance and yield stiffness of BRSPSWs

4.3.2. Influence column's width-to-thickness ratio

During applying the lateral cyclic load on steel tubes infilled by concrete, the section's webs are parallel to the loading direction, and the flanges are perpendicular to the loading direction (see Fig. 18). Thus, the flanges will be under high stress and are more probably to buckle during the loading process. The width-to-thickness obviously influenced the seismic behavior of BRSPSWs. According on AISC-360, the CFT columns is classified as a compact section when the ratio is $D/t < 2.26\sqrt{E_s / f_y}$, indicating that the steel section tends to yield before bucking and provide a good confinement to the concrete infill. Therefore, all cases in this section belong to a compact section.

The FE-model of BRSPSW-2 was taken as the basic model the width-to-thickness ratio is $\boldsymbol{D/t = 13.3\%}$. However, various FE models have different D/t values as follows: *10%, 11.4, 13.3, 16%* and *20%* by changing the column's thickness. The comparison of hysteretic and skeleton curves is illustrated in Fig. 19(a-b). It is noted that initial stiffness and ductility remained almost stable. Fig. 19(c) represents the effect of D/t ratio on the lateral resistance and yield stiffness. Both yield and peak lateral resistance showed a slight increase with decreasing the D/t ratio. Also, it can be noticed that the ratio of yield-to-peak lateral resistance tended to decline when D/t was reduced. On the other hand, the lateral yield stiffness declined within reducing D/t ratio due to less resistance offered by steel tubes. Finally, D/t ratio shows a minor effect on the cyclic behavior of BRSPSWs.

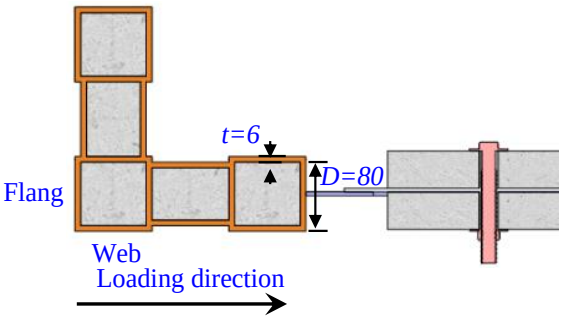

Fig. 18 Column's section and loading direction

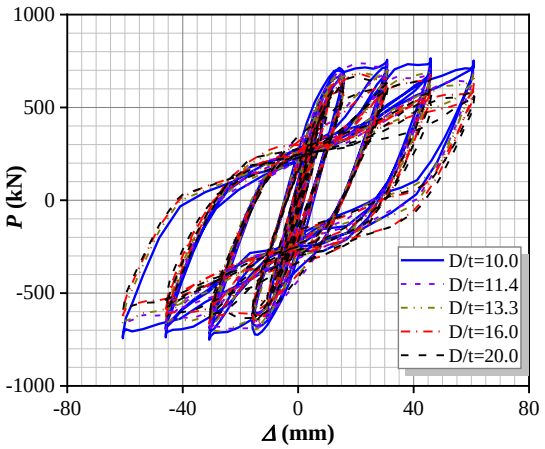

(a) Comparison of hysteretic curves

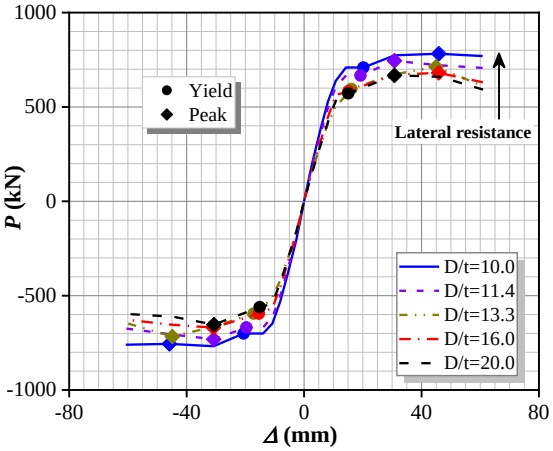

(b) Comparison of skeleton curves

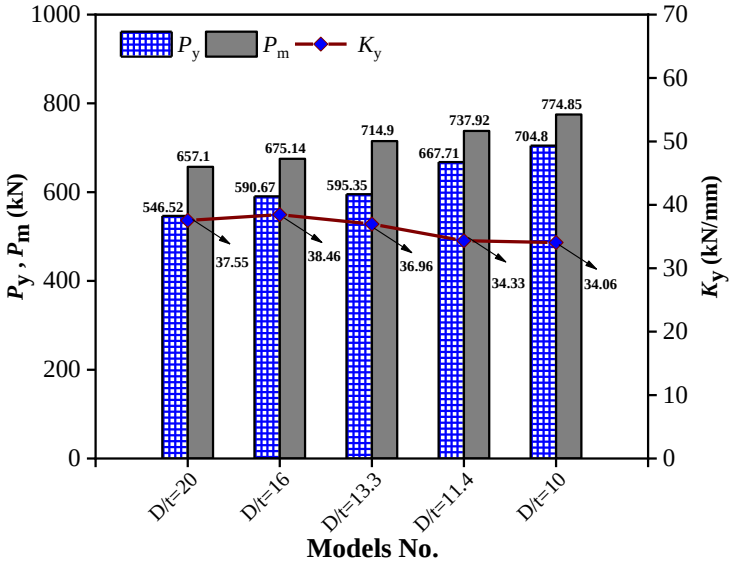

(c) Comprehensive comparison of lateral resistance and yield stiffness

Fig. 19 Impact of width-to-thickness ratio of column on lateral resistance and yield stiffness of BRSPSWs

4.3.3. Influence of axial compression ratio

Regarding the test program, the initial step includes the applying of axial compression load, which is then pursued by horizontal loading. Noticeable, it was found in the literature that the cyclic behavior of wall structures is significant by axial compression ratio [48-50]. Due to the limitation of equipment in the laboratory, there was no axial compression ratio (n_d) applied. Thus, the axial compression ratio was considered during FE-simulation with *0%*, *25%*, *50%*, *75%* and *100%* axial compression.

Fig. 20 (a-b). compares the load-displacement responses, involving hysteretic and skeleton with varying axial compression ratios. It is clear that the models behaved linearly in the initial stage, and the ductility was greatly affected by the axial compression ratio. When the axial compression ratio was 100%, the model was exposed to hard damage, so it could not complete to the end. In contrast, yield and peak lateral showed an enormous decreased trend when the axial compression ratio increased, as illustrated in Fig. 20(c). Besides, the ratio of yield-to-peak resistance went up with rising the axial compression ratio. Similarly, the yield stiffness was declined with rising the axial compression ratio. Finally, the cyclic behavior of BRSPSW is dramatically influenced by the axial compression ratio.

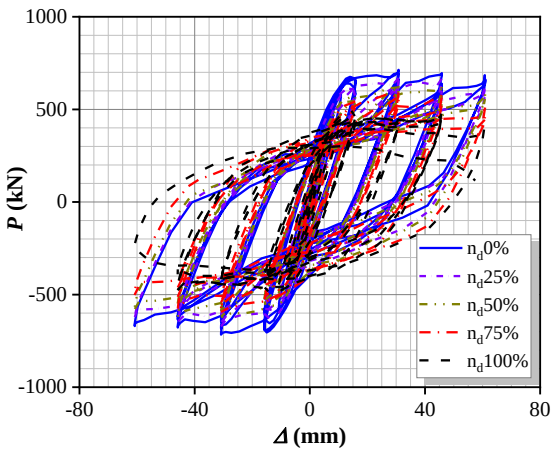

(a) Comparison of hysteretic curves

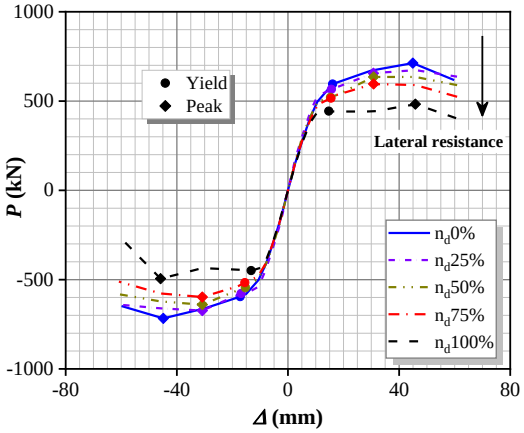

(b) Comparison of skeleton curves

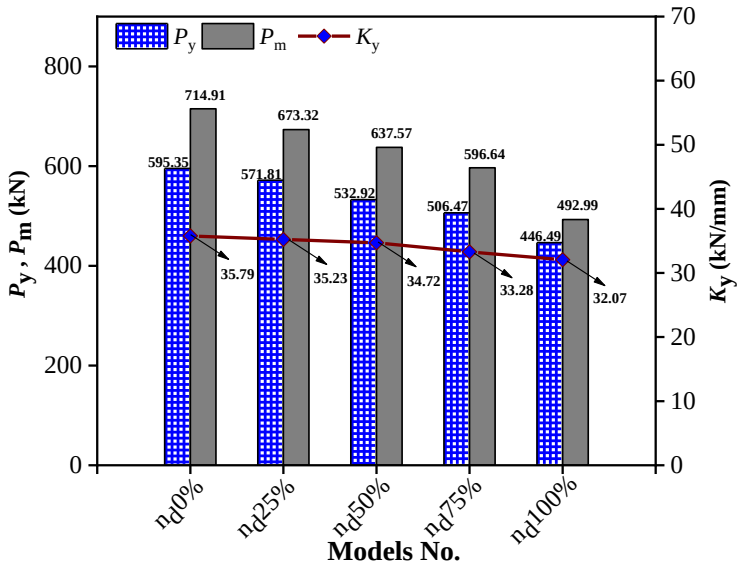

(c) Comprehensive comparison of lateral resistance and yield stiffness

Fig. 20 Impact of axial compression load ratio on lateral resistance and yield stiffness of BRSPSWs

4.3.4. Influence of height-to-thickness ratio of inner steel plate

The size of the inner steel plate has an important impact in determining not only the occurrence of local buckling but also the seismic behavior of BRSPSWs in their entirety. The categorization of BRSPSWs into thick and thin types is determined by the ratio of their inner steel plate's height to their thickness (H_p/t_s), as seen in Fig. 21. When the H_p/t_s ratio of the inner steel plate is small, thicker steel plate tend to buckle after yield, and fully utilize their lateral stiffness. Oppositely, thin steel plate has a bigger height-to-thickness ratio, they tend to buckle earlier than reaching their yield point. According to JGJ/J 380-2015 [51], the H_p/t_s ratio of BRSPSW should be between $100 < H_p / t_s\sqrt{235/f_y} < 600$. As the tested sample has a thickness of 4mm, it can be categorized as a thin steel plate, which tends to undergo buckling prior to exhibiting yielding behavior.

During the test and FE-analysis, it was found out that the local buckling appeared diagonally in the tension field and developed into overall buckling (see Fig. 16). To investigate the impact of the height-to-thickness ratio, five models were conducted with different thicknesses of inner steel plate (t_s=*2 mm ; 3 mm ;4 mm ; 5 mm* and *6 mm*). Fig. 22(a-b). The graph illustrates the modified thicknesses of the inner steel plate by plotting both hysteretic and skeleton responses, dramatically affecting the initial stiffness. Besides, it observed that the ductility declined with reducing the thickness of inner steel plates of because of damaged inner steel plates when the thickness of the inner steel plates is smaller. The hysteretic also could not complete all loops compared with the larger thickness. In addition, the inner steel plates' thickness also has a considerable consequence on lateral resistance and stiffness, as displayed in Fig. 22. the yield and peak lateral resistance were increased sharply with rising the thickness of inner steel plates, while the ratio of yield-to-peak was declined (see. Fig. 22(c)). In the same vein, the lateral yield stiffness showed a sharp increment. Consequently, the heigh-to-thickness ratio significantly impacts the overall seismic performance BRSPSWs.

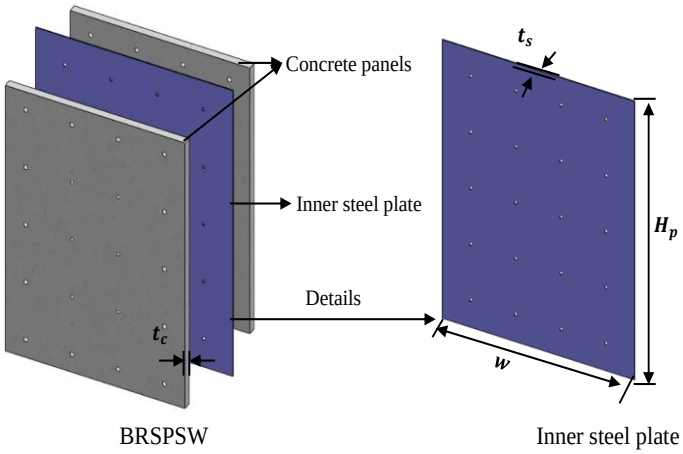

Fig. 21 Details of inner steel plate

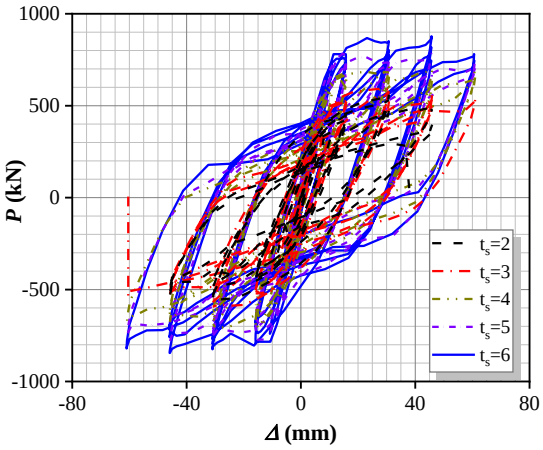

(a) Comparison of hysteretic curves

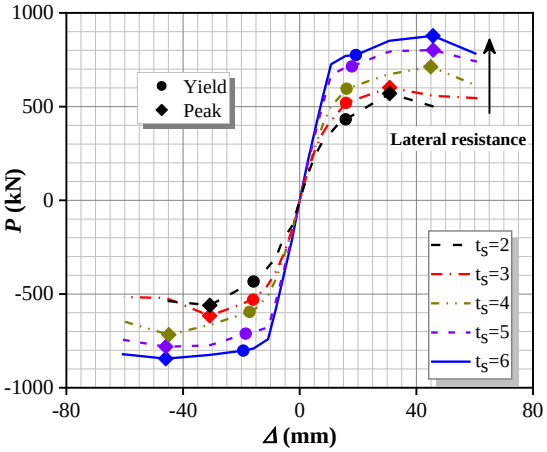

(b) Comparison of skeleton curves

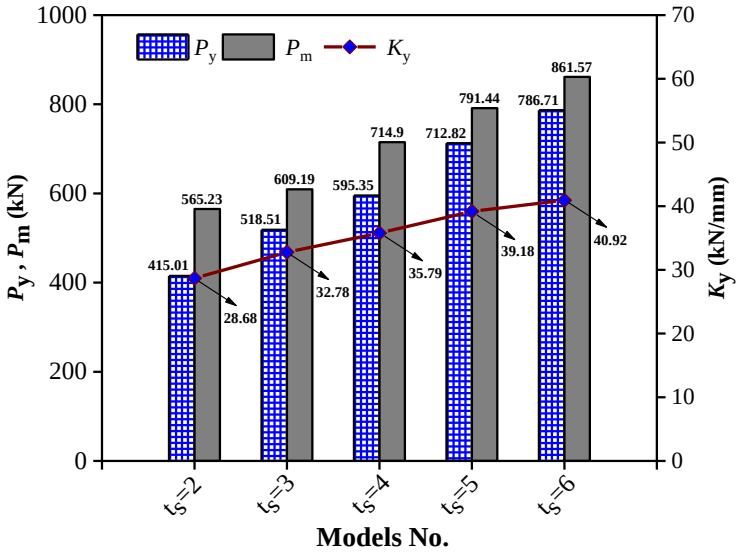

(c) Comprehensive comparison of lateral resistance and yield stiffness

Fig. 22 Impact of height-to-thickness of inner steel plates ratio on lateral resistance and yield stiffness of BRSPSWs

4.3.5. Influence concrete panel's thickness

In the tested specimens, the concrete panel thickness was considered as ($t_c = 40mm$), and it was observed the concrete panel's thickness contributed greatly to reducing local buckling of inner steel plates. For this reason, five concrete panel's thicknesses from 20mm to 100mm with 20 intervals were modeled to study the impact of this parameter. The results showed that the concrete panel's thickness impacted minimally on the initial stiffness and ductility. Rising the thickness of concrete panels increased the initial stiffness and decreased ductility, and the pinch behavior of hysteretic curves tended to be less with increasing the lateral displacement due to limiting of inner steel plate's buckling, as demonstrated in Fig. 23(a-b). Additionally, the lateral resistance and yield stiffness went up steadily, increasing the thickness of concrete panels, as seen in Fig. 23(c). Besides, there was no change in yield-to-peak lateral resistance. Thus, rising the of concrete panels's thickness increased the lateral resistance and stiffness but reduced the ductility. Accordingly, concrete thickness has a minor factor in the overall seismic behavior of BRSPSWs.

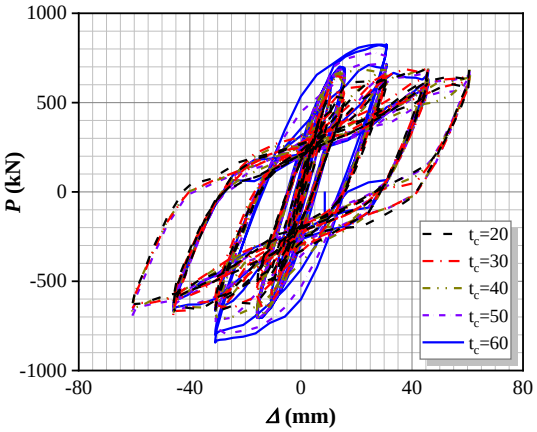

(a) Comparison of hysteretic curves

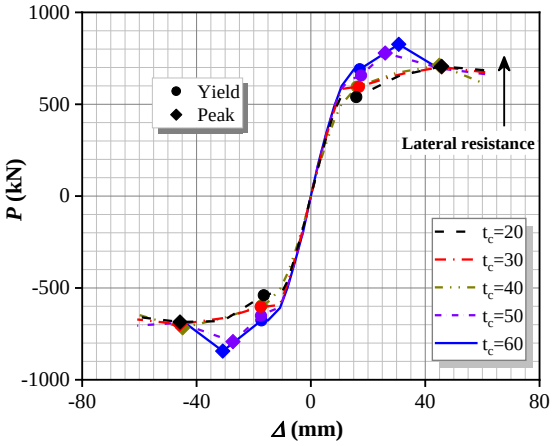

(b) Comparison of skeleton curves

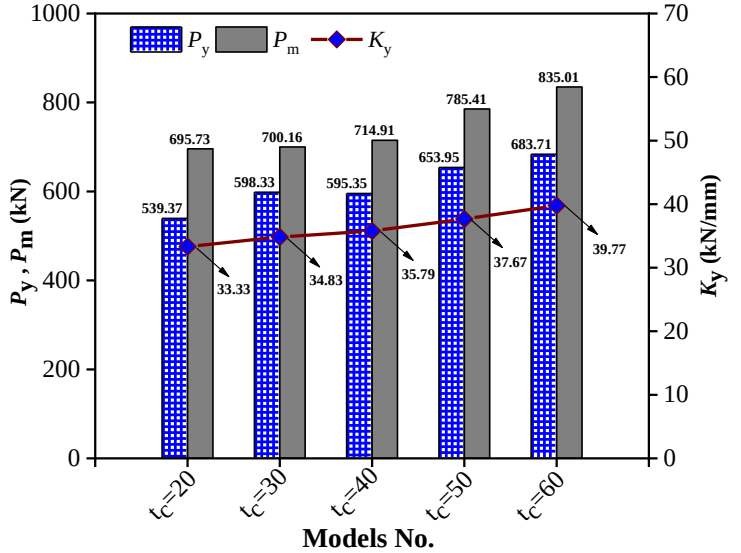

(c) Comprehensive comparison of lateral resistance and yield stiffness

Fig. 23 Effect concrete panels' thickness on lateral resistance and yield stiffness of BRSPSWs

4.3.6. Influence of bolt arrangements

During the fabrication process, the inner steel plates were connected to concrete panels using high-strength bolts arranged in four rows and five columns (B4x5) at equal intervals (see Fig. 21). Based on test and FE-simulation results, concrete cracking appeared firstly on the concrete panels' holes, followed by buckling on inner steel plates. Therefore, five models were established in FE simulation to investigate the effect of bolt arrangements (*B4x5; B4x3; B4x2; B2x3;* and *B4x2*). The result showed that various bolts with different arrangements have approximately no effect on initial stiffness and ductility (see Fig. 24). On the other hand, this factor greatly affected the overall steel plates' buckling and the cracking of concrete panels. Increasing the number of row of bolts can obviously restrain the out-plane buckling of inner steel plates and concrete panels while increasing the number of columns of bolts could not resist, as shown in Fig. 25(a-e). To sum up, the bolt arrangements do not have a great effect on lateral resistance, stiffness and ductility, but it has a substantial impact on the buckling behavior of the inner steel plates and cracking of concrete.

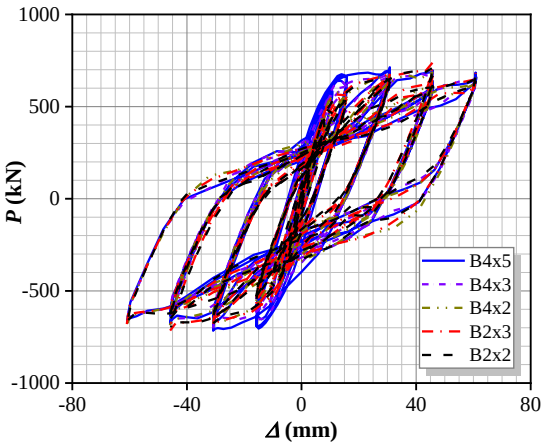

(a) Comparison of hysteretic curves

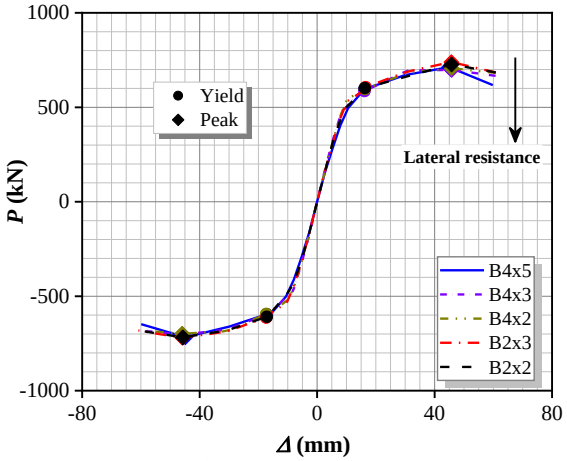

(b) Comparison of skeleton curves

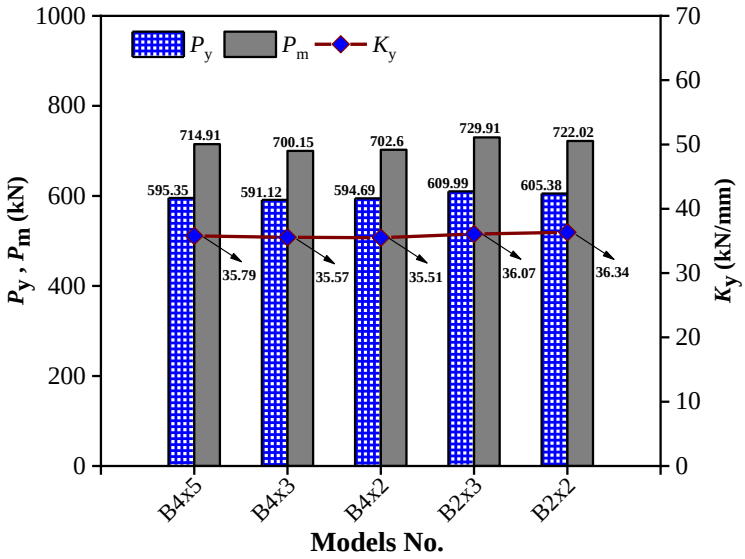

(c) Comprehensive comparison of lateral resistance and yield stiffness

Fig. 24 Effect bolts arrangments thickness on lateral resistance and yield stiffness of BRSPSWs

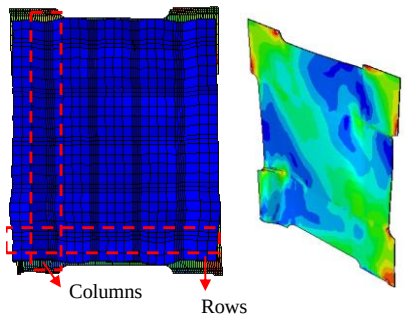

(a) B4x5

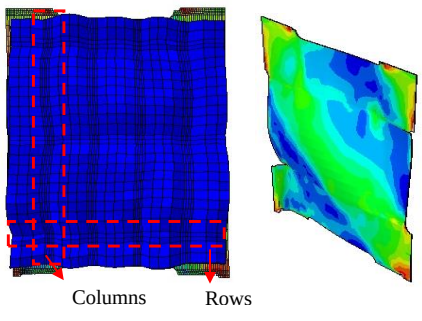

(b) B4x3

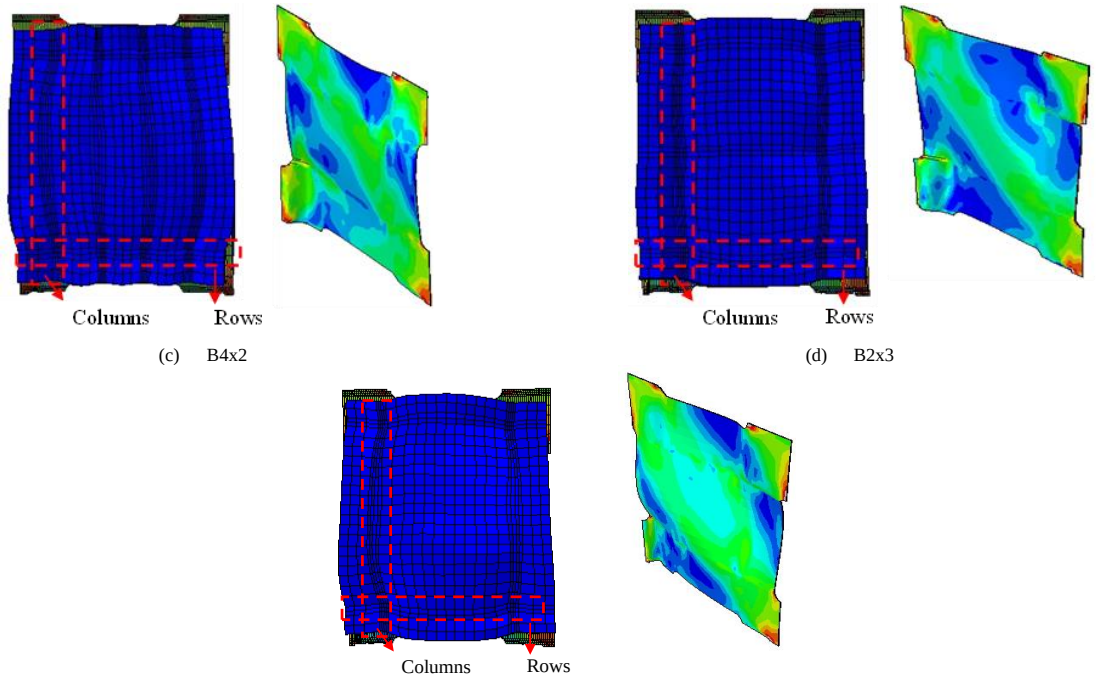

(c) B4x2 (d) B2x3

(e) B2x2

Fig. 25 Effect of bolt arrangements on out-plane deformation of BRSPSWs

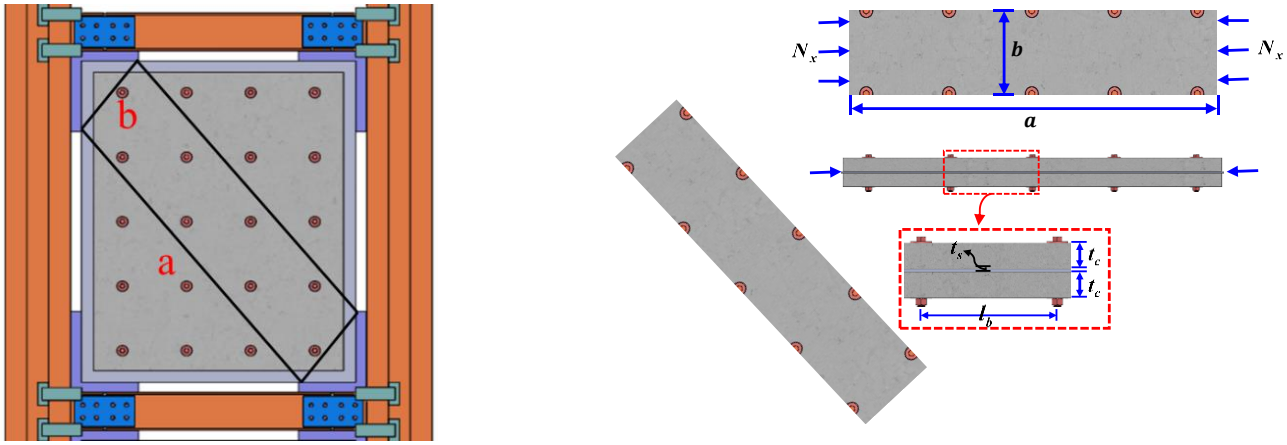

(a) Partially connected BRSPSW (b) Simplified method for calculating the lateral resistance

Fig. 26 Buckling response of the inner steel plate and simplified calculation lateral resistance

4.4. Discussions

The parametric analyses represent that [1] modifying the length leg that connected to the steel plate increases the yield and peak lateral resistance 28 %, and 30%. It also reduces the yield stiffness by roughly and 18%. [2] By raising the column's width-to-thickness ratio from 10% to 20%, there is an improvement in both yield and peak lateral resistance by approximately 26% and 16%, respectively. However, this change leads to a reduction in the yield stiffness by about 5%. [3] increasing the axial compression ratio from 0% to 100% results in a decrease of approximately 25% in the yield, 31% in the peak lateral resistance, and 10% in the yield stiffness. [4] By elevating the thickness of the steel plate from 2 mm to 6 mm, there is a substantial increase in both the yield and peak lateral resistance by approximately 62% and 42%, respectively, along with a boost in the yield stiffness by about 34%. [5] Changing the concrete panel's thickness of the from 20 mm to 60 mm, there is an increase in both the yield and peak lateral resistance by approximately 24% and 20%, respectively, along with an increase in the yield stiffness by about 18%. [6] Changing the bolts arrangement does not affect lateral resistance and yield stiffness but it greatly affects the inner steel plates' buckling behavior.

Accordingly, the most efficient method for enhancing the lateral resistance and yield stiffness is by increasing steel plate's thickness. In contrast, the leg's length of the steel plate and concrete thickness have a less significant factor on improving the lateral resistance and yield stiffness compared to the thickness of the steel plate. On the other hand, expanding the axial compression ratio resulted in reduction on the lateral resistance and yield stiffness. The width-to-thickness ratio has an excellent contribution on improving lateral resistance but reducing yield stiffness value but reducing. Finally, the steel plate's buckling behavior is improved by the configuration of bolts that connects the concrete panels and inner steel plates.

5. Theoretical model on the lateral resistance of BRSPSWs

In accordance with test and FE modeling findings, it was founded that the bearing capacity was mainly calculated by steel plate and frame. Therefore, a calculation approach was suggested to estimate the lateral resistance based on plate-frame interaction theory, which was firstly introduced by Sabouri et al. [52]. This method predicted the lateral resistance for SPSW with L-shaped columns in ref [47]. The previous research on PFI theory only considered the contribution of the steel plate and frame elements; however, the parametric studies in this paper showed that the inner steel plate's buckling-restrained using concrete panels has a minor effect on the wall's lateral resistance. Subsequently, the calculation equations were assumed based on PFI theory, and then it was modified to consider the buckling restrained by the concrete panels. On the other hand, the effect of bolt arrangements is ignored due to approximately zero effect based on FE analysis. Therefore, the following assumption can be drawn:

$$P_{MPFI} = P_s + P_f \tag{16}$$

where P_{MPFI} indicates the peak lateral resistance of the BRSPSWs, P_s and P_f denote the peak lateral resistance of the inner steel plate and frame, respectively.

(1) As the inner steel plate's local buckling happened diagonally, it can be simplified as length (a) and width (b), as illustrated in Fig. 26. In accordance with stability of the steel plate, the buckling strength can be determined as

$$N_x = \frac{\pi^2 D_s}{a^2}(m + \frac{1}{m}\frac{a^2}{b^2})^2 \tag{17}$$

In this context, the variable " N_x " represents the amount of compressive load per unit height applied to the "b" side, "m" denotes the quantity of half-wavelengths of buckling in the "a" direction, and " D_s " refers to the out-of-plane flexural rigidity of the steel plate, expressed as

$$D_s = \frac{E_s t_s^3}{12(1-\nu_s^2)} \tag{18}$$

where E_s stands for modulus of elasticity; t_s stands for steel plates' the thickness; ν_s is the Poisson's ratio.

It is noteworthy to mention that the steel plate exhibited diagonal buckling with a longer wavelength, which is primarily influenced by the bolt spacing and the types of the connection linking the frame elements to steel plates. However, the buckling response will reproduce to a short wavelength since it reduces with increasing compressive force, as shown in Fig. 27. Consequently, the bending moment of the steel plate and plastic hinges form at the wave peak. The longitudinal and transversal displacement, (γ and δ) can be drawn in term of the buckling wave rotation as follows:

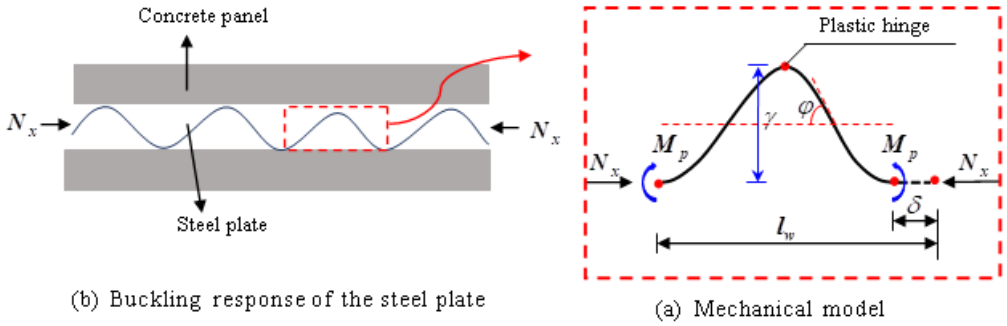

Fig. 27 Equavilent model of steel plate's buckling

$$\delta = \frac{8\gamma^2}{l_w} \tag{19}$$

where l_w refers to the inner steel plate's half-wavelength of buckling; φ is buckling wave's the rotation angle. The compressive resistance of the steel plate's the buckling is illustrated in Fig. 27. And it can be expressed as:

$$N_x = \frac{2\sqrt{2}M_p}{bl_w}\frac{1}{\sqrt{\varepsilon_s}} \tag{20}$$

where ε_s stands for the nominal strain of the steel plate; M_p stands for the plastic moment of the steel plate which is determined as follows.

$$M_p = \frac{bt_s^2}{4} f_y \tag{21}$$

In Fig. 28, the steel plate and concrete panels were simplified to equivalent braces. To apply the lateral load at the pinnacle of the equal braced framework, the following expression can be utilized.

$$P_s = (f_y + \sigma_x) A_e \cos\alpha \tag{22}$$

where f_y refers to the yield strength of the inner steel plate $\sigma_x = N_x / t_s$ refers to the high-order buckling the resistance of the inner steel plate, $A_e = (\sqrt{L_p^2 + H^2}/4) t_s$ is the efficient region of equivalent braces (see Fig. 28). The AISC-360 code [53]can be utilized to calculate the angle of inclination (α) for the tension field and as follows:

$$tan\alpha = \sqrt{\frac{1 + \frac{t_s L_p}{2A_c}}{1 + t_s H(\frac{1}{A_b} + \frac{H^3}{360 I_c L_p})}} \tag{23}$$

where t_s is the thickness of plate, L_p is the leg's length, A_c is the equivalent area of the column, h refers to floor's height of the, A_b refers to beam's the cross-sectional, I_c is the moment of inertia of the column.

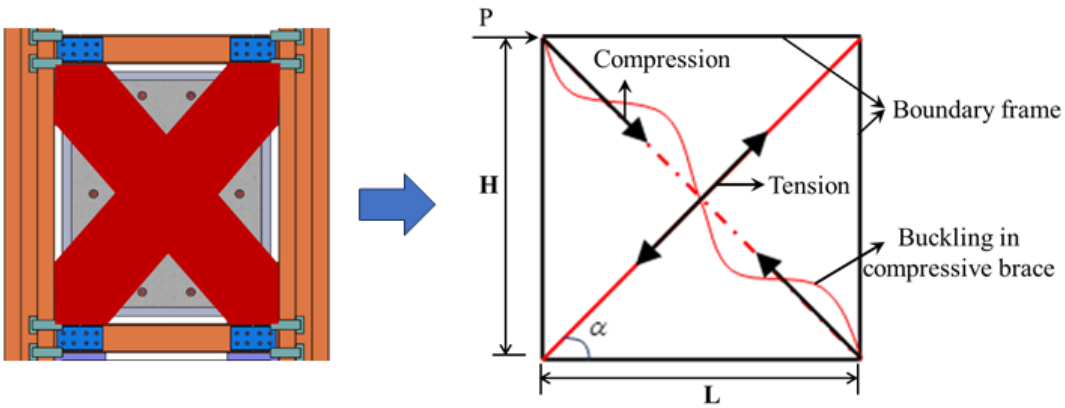

Fig. 28 Simplified and Equivalent model for the frame buckling-restained steel plate shear wall

(2) The lateral resistance of the frame can be computed using the following formula.

$$P_f = \frac{4(M_f - \varphi n_d N_d e)}{H} \quad (24)$$

where M_f is the plastic moment, and it can be calculated using the equation presented in Ref [54]; φ is coefficient factor (0.75) in the case; n_d is the axial compression ratio; N_d is the design compression load; e is the eccentric distance based on neutral axis as shown in Fig. 29.

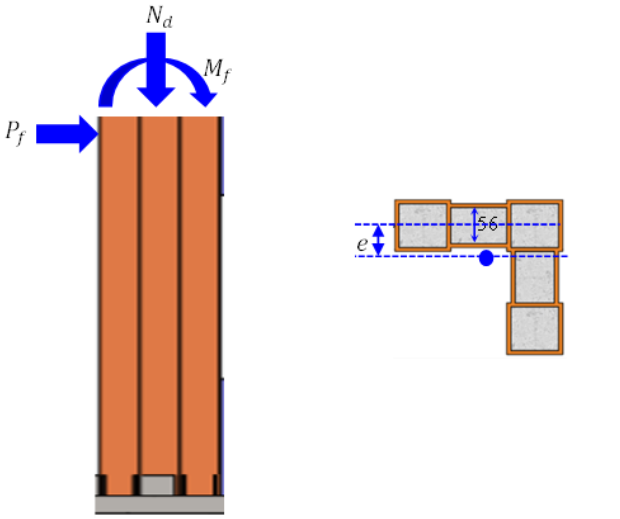

Fig. 29 Calcaution diagram of frame's columns subjected to combained compression and horizontal load

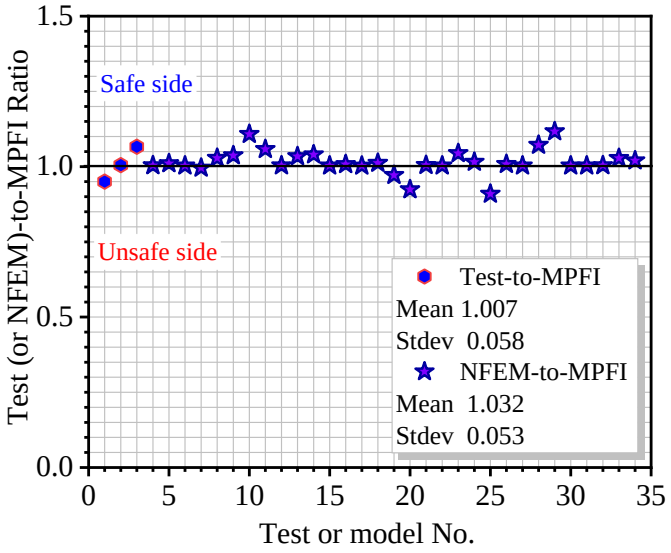

Fig. 30 Scatter of test and NFEM to MPFI predication ratio

5.1. Verification

The calculation method results for yield lateral resistance of BRSPSWs were firstly compared with test results and then with numerical results. The MPFI prediction showed high agreement with the test and numerical results, as shown in Fig. 30. Besides, most of the MPFI results were on the safe side, ramming this method could be used for the design approach of BRSPSWs with L-shaped CFT columns.

6. Conclusion

This paper firstly developed nonlinear finite element models (NFEM) for L-shaped CFT columns frame-buckling-restrained steel plate shear walls (BRSPSWs). After verifying the FE models, through parametric studies, the effect of various factors on the lateral resistance and yield stiffness was assessed. Then based on plate-frame interaction (PFI) theory, a modified MPFI was proposed to calculate the yield lateral resistance. The main conclusions of this study can be drawn as follows:

(1) The seismic performance of frame BRSPSWs was investigated through FE models. Failure modes, hysteretic and skeleton curves were compared with tested results, and the FE models could accurately predicate the seismic behavior of BRSPSWs. In addition, the test-to-FE prediction ratio showed high accuracy for yield, peak lateral resistance, and yield stiffness.

(2) Increasing the leg's length from 150 mm to 400 mm leads to about 28 %, 30 % and 18% increase in yield, peak lateral resistance, and yield stiffness. On the other hand, rising the thickness of the steel plates from 2 mm to 6 mm takes increment by about 62 %, 42 % and 34 %, yield and peak lateral resistance and yield stiffness. Therefore, modification on steel plates significantly affects the overall behaviors of BRSPSWs, whether in leg length or thickness.

(3) The yield and peak lateral resistance and yield stiffness were reduced by roughly 25 %, 31 % and 10%, with declining the axial compression ratio increases from 0% to 100%. Thus, the axial compression ratio minimally affects the lateral resistance and stiffness. However, increasing the width-to-thickness ratio of the columns raises the yield and peak lateral resistance and yield stiffness by about 26 %, 16 %, but it declines the stiffness by about 25 %. Thus, this parameter can be ignored during the design of the BRSPSWs.

(4) Changing the concrete panel's thickness from 20 mm to 60 mm booms the yield and peak lateral resistance and stiffness by about 24 %, 20 % and 18 %, respectively, and it greatly impacts lateral displacement ductility, which is uncoverable on seismic design of BRSPWS system. Thus, the concrete thickness slightly impacts the structural behavior of BRSPSWs. Oppositely, the lateral resistance and stiffness of concrete panels connected to steel plates remain unaffected by the number of bolts used. However, buckling can be prevented by increasing the number of rows of bolts.

(5) A modified plate-frame interaction approach has been suggested to estimate the yield lateral resistance. Then the predicted outcomes are verified to the test and FE models' results to verify it, and they showed a good agreement against FE results.

Acknowledgment

This work is sponsored by the National Key Research and Development Project (Grant No. 2019YFD1101005). The Guangdong Basic and Applied Basic Research Foundation (Nos. 2020A1515110304）

Nomenclature

f_y	yield strength of steel	L_p	leg's length
f_u	ultimate strength of steel	n_d	axial compression ratio
E_s	steel elastic modulus	H_p / t_s	height-to-thickness ratio of inner steel plates
σ_s	stress of steel	t_c	concrete panels' thickness
$\varepsilon_e, \varepsilon_{e1}, \varepsilon_{e2}$	intermediate strain	$(B(RxC))$	bolt arrangements
ε_{e3}	ultimate strain	P_{MPFI}	prediction of peak lateral resistance
A_s	cross-sectional of steel	P_{ms}	lateral resistance of the steel plate

f_{cu}, f_c	cube and cylinder compressive strength of concrete	P_{mf}	lateral resistance of the frame
E_c	concrete elastic modulus	A_e	equivalent area of braces
A_c	cross-sectional of concrete	N_x	high order buckling resistance of the steel plate
σ_{c0}	compressive stress concrete	α	inclination angle of the tension filed
ε_{c0}	strain of concrete at f_c	**Abbreviation**	
ν	Poisson's ratio	BRSPSWs:	Buckling-restrained steel plate shear walls
σ_{t0}	tensile stress concrete	SPSWs:	Steel plate shear walls
ε_{t0}	strain of concrete at σ_{t0}	PFI:	Nonlinear finite element model
P_y	yield lateral resistance	NFEM:	Plate-frame interaction
P_m	peak lateral resistance	MPFI:	Modified Plate-frame interaction
K_y	yield lateral stiffness	CFT:	Concrete-filled steel tube
Δ_y	yield displacement	CDPM:	Concrete damage plasticity model
D/t	columns' width-to-thickness		

Reference

[1] Y. Takahashi, Y. Takemoto, T. Takeda, and M. Takagi, "Experimental study on thin steel shear walls and particular bracings under alternative horizontal load," in *Preliminary Report, IABSE, Symp. On Resistance and Ultimate Deformability of Tsructures Acted on by Well-defined Repeated Loads, Lisbon, Portugal*, 1973.

[2] L. Thorburn, G. Kulak, and C. Montgomery, "Analysis of steel plate shear walls, Structural Engineering Report No. 107," *Edmonton, Alberta: University of Alberta, Department of Civil Engineering*, 1983.

[3] E. W. Tromposch and G. L. Kulak, "Cyclic and static behaviour of thin panel steel plate shear walls," 1987.

[4] V. Caccese, M. Elgaaly, and R. Chen, "Experimental study of thin steel-plate shear walls under cyclic load," *journal of Structural Engineering*, vol. 119, no. 2, pp. 573-587, 1993.

[5] R. Driver, "Seismic behavior of steel plate shear walls [Dissertation of Ph. d.]," *D. Department of Civil and Environmental engineering, University of Alberta, Alberta, Canada*, 1997.

[6] H.-G. Park, J.-H. Kwack, S.-W. Jeon, W.-K. Kim, and I.-R. Choi, "Framed steel plate wall behavior under cyclic lateral loading," *Journal of structural engineering*, vol. 133, no. 3, pp. 378-388, 2007.

[7] A. Astaneh-Asl, *Seismic behavior and design of steel shear walls*. Structural Steel Educational Council Moraga, CA, 2001.

[8] A. Astaneh-Asl, *Seismic behavior and design of composite steel plate shear walls*. Structural Steel Educational Council Moraga, CA, 2002.

[9] Q. Zhao and A. Astaneh-Asl, "Cyclic behavior of traditional and innovative composite shear walls," *Journal of Structural Engineering*, vol. 130, no. 2, pp. 271-284, 2004.

[10] L. Ye, L. Guoqiang, and S. Feifei, "Experimental study on buckling-restrained composite steel plate shear wall with large aspect ratio," *Progress in Steel Building Structures*, vol. 11, no. 2, pp. 18-27, 2009.

[11] S.-J. Chen and C. Jhang, "Cyclic behavior of low yield point steel shear walls," *Thin-walled structures*, vol. 44, no. 7, pp. 730-738, 2006.

[12] J. W. Berman and M. Bruneau, "Experimental investigation of light-gauge steel plate shear walls," *Journal of Structural Engineering*, vol. 131, no. 2, pp. 259-267, 2005.

[13] T. M. Roberts and S. Sabouri-Ghomi, "Hysteretic characteristics of unstiffened perforated steel plate shear panels," *Thin-Walled Structures*, vol. 14, no. 2, pp. 139-151, 1992.

[14] I.-R. Choi and H.-G. Park, "Steel plate shear walls with various infill plate designs," *Journal of structural engineering*, vol. 135, no. 7, pp. 785-796, 2009.

[15] T. Hitaka, C. Matsui, and J. i. Sakai, "Cyclic tests on steel and concrete-filled tube frames with Slit Walls," *Earthquake engineering & structural dynamics*, vol. 36, no. 6, pp. 707-727, 2007.

[16] S. Jin, J. Ou, and J. R. Liew, "Stability of buckling-restrained steel plate shear walls with inclined-slots: theoretical analysis and design recommendations," *Journal of Constructional Steel Research*, vol. 117, pp. 13-23, 2016.

[17] Q. Liu, G. Li, and Y. Lu, "Experimental and theoretical study on the steel bound-columns with buckling restrained steel plate shear wall," in *Proceedings of the EUROSTEEL, 7th European conference on steel and composite structures, Italy*, 2014.

[18] M.-W. Wei, J. R. Liew, Y. Du, and X.-Y. Fu, "Seismic behavior of novel partially connected buckling-restrained steel plate shear walls," *Soil Dynamics and Earthquake Engineering*, vol. 103, pp. 64-75, 2017.

[19] M.-W. Wei, J. R. Liew, M.-X. Xiong, and X.-Y. Fu, "Hysteresis model of a novel partially connected buckling-restrained steel plate shear wall," *Journal of Constructional Steel Research*, vol. 125, pp. 74-87, 2016.

[20] M.-W. Wei, J. R. Liew, and X.-Y. Fu, "Panel action of novel partially connected buckling-restrained steel plate shear walls," *Journal of Constructional Steel Research*, vol. 128, pp. 483-497, 2017.

[21] M.-W. Wei, J. R. Liew, D. Yong, and X.-Y. Fu, "Experimental and numerical investigation of novel partially connected steel plate shear walls," *Journal of Constructional Steel Research*, vol. 132, pp. 1-15, 2017.

[22] Y. Du, Y. Zhang, T. Zhou, Z. Chen, Z. Zheng, and X. Wang, "Experimental and numerical study on seismic behavior of SCFRT column frame-buckling restrained steel plate shear wall structure with different connection forms," *Engineering Structures*, vol. 239, p. 112355, 2021.

[23] Y. Guo and Q. Dong, "Static behavior of buckling-restrained steel plate shear walls," in *Tall Buildings: From Engineering to Sustainability*: World Scientific, 2005, pp. 666-670.

[24] W.-Y. Liu, G.-Q. Li, and J. Jiang, "Mechanical behavior of buckling restrained steel plate shear walls with two-side connections," *Engineering Structures*, vol. 138, pp. 283-292, 2017.

[25] H. Gao and G. Li, "Experimental and theoretical study on composite steel plate shear walls," Master's Dissertation, Tongji University, Shanghai, China, 2007.

[26] F. Sun, H. Gao, and G. Li, "Experimental research on two-sided composite steel plate walls," in *Proceeding of the 4th technical seminar on steel structure for Cross-Strait and Hong Kong. Tongji University Press, Shanghai, China*, 2006.

[27] Z.-S. Huang, Z.-Z. Yin, and B.-Y. Song, "STUDY ON SEISMIC BEHAVIOR OF TRAPEZOIDAL CORRUGATED STEEL PLATE SHEAR WALL STRUCTURE WITH PEC COLUMN," *ADVANCED STEEL CONSTRUCTION*, vol. 19, no. 2, pp. 157–165, 2023.

[28] L. Guo, Q. Rong, X. Ma, and S. Zhang, "Behavior of steel plate shear wall connected to frame beams only," *International Journal of Steel Structures*, vol. 11, no. 4, pp. 467-479, 2011.

[29] A. Pirmoz, "Beam-attached steel plate shear walls," *The Structural Design of Tall and Special Buildings*, vol. 21, no. 12, pp. 879-895, 2012.

[30] M. Wang, W. Yang, Y. Shi, and J. Xu, "Seismic behaviors of steel plate shear wall structures with construction details and materials," *Journal of Constructional Steel Research*, vol. 107, pp. 194-210, 2015.

[31] B. Jkta, A. Xhz, N. B. Xin, A. Yhw, and W. A. Kang, "Experimental and numerical investigation of cross-shaped buckling-restrained SPSWs with composite structure," *Journal of Building Engineering*, vol. 47 (2022) 103873, 2021.

[32] C. Zhihua, "New-Type special-shaped column by steel structure and composite " *Steel Construction*, vol. 2, pp. 27-29, 2006.

[33] Q.-Q. Xiong, W. Zhang, Z.-H. Chen, T. Zhou, and J.-H. Qian, "EXPERIMENTAL STUDY ON THE BEHAVIOUR OF L-SHAPED COLUMNS FABRI-CATED USING CONCRETE-FILLED STEEL TUBES UNDER ECCENTRIC LOADS," *ADVANCED STEEL CONSTRUCTION*, vol. 18, no. 2, pp. 528-535, 2022.

[34] T.-F. Ma, Z.-H. Chen, K. Khan, and Y.-S. Du, "EXPERIMENTAL AND NUMERICAL ANALYSIS OF L-SHAPED COLUMN COMPOSED OF RECYCLED AGGREGATE CONCRETE-FILLED SQUARE STEEL TUBES UNDER ECCENTRIC COMPRESSION," *ADVANCED STEEL CONSTRUCTION*.

[35] Z.-h. Chen, Z.-y. Li, B. Rong, and X.-l. LIU, "Experiment of axial compression bearing capacity for crisscross section special-shaped column composed of concrete-filled square steel tubes," *Journal of Tianjin University*, vol. 39, no. 11, pp. 1275-1282, 2006.

[36] Z.-h. Chen, B. Rong, and A. Fafitis, "Axial compression stability of a crisscross section column composed of concrete-filled square steel tubes," *Journal of Mechanics of Materials and Structures*, vol. 4, no. 10, pp. 1787-1799, 2010.

[37] Z.-H. Chen, R. Ma, Y.-S. Du, and M. Lian, "Experimental and Theoretical Research on Rcft Beam-Columns Fabricated with Q420b High-Strength Steel Subjected To Eccentric Load," *ADVANCED STEEL CONSTRUCTION*, vol. 16, no. 4, pp. 287-296, 2020.

[38] T. Zhou, Y. Jia, M. Xu, X. Wang, and Z. Chen, "Experimental study on the seismic performance of L-shaped column composed of concrete-filled steel tubes frame structures," *Journal of Constructional Steel Research*, vol. 114, pp. 77-88, 2015.

[39] "GB/T 228.1-2010 Tensile testing of metallic materials - Part 1: room temperature test method[S], Standards press of China, Beijing," 2011 (In Chinese).

[40] *GB/T 50081, Ordinary Concrete Mechanices Performance Test Method Standard, 2019*. (In Chinese).

[41] *JGJ/T101, Specification for Seismic Test of Building, 2015, (in Chinese)*.

[42] D. S. Simulia, "ABAQUS 6.13 User's manual," *Dassault Systems, Providence, RI*, vol. 305, p. 306, 2013.

[43] F. H. Aboutalebi and A. Banihashemi, "Numerical estimation and practical validation of Hooputra's ductile damage parameters," *The International Journal of Advanced Manufacturing Technology*, vol. 75, no. 9-12, pp. 1701-1710, 2014.

[44] *Concrete Filled Steel Tubular Structures-Theory and Practice (Third Edition)* L. Han, Beijing: Sicence press, 2016 (in Chinese).

[45] A. A. Standard, "Building Code Requirements for Structural Concrete (ACI 318-11)," in *American Concrete Institute*, 2011.
[46] Z. Wang, J.-B. Yan, and X.-M. Liu, "NUMERICAL AND THEORETICAL STUDIES ON DOUBLE STEEL PLATE COMPO-SITE WALLS UNDER COMPRESSION AT LOW TEMPERATURES," *ADVANCED STEEL CONSTRUCTION*, 2019.
[47] K. Wang, M.-N. Su, Y.-H. Wang, J.-K. Tan, H.-B. Zhang, and J. Guo, "Behaviour of buckling-restrained steel plate shear wall with concrete-filled L-shaped built-up section tube composite frame," *Journal of Building Engineering*, vol. 50, p. 104217, 2022.
[48] B. Zhao *et al.*, "Experimental seismic behavior of SCFRT column chevron concentrically braced frames," *Journal of Constructional Steel Research*, vol. 133, pp. 141-155, 2017.
[49] Z. Chen, H. Xu, Z. Zhao, X. Yan, and B. Zhao, "Investigations on the mechanical behavior of suspend-dome with semirigid joints," *Journal of Constructional Steel Research*, vol. 122, pp. 14-24, 2016.
[50] Z. Zhao, Z. Chen, X. Yan, H. Xu, and B. Zhao, "Simplified numerical method for latticed shells that considers member geometric imperfection and semi-rigid joints," *Advances in Structural Engineering*, vol. 19, no. 4, pp. 689-702, 2016.
[51] "JGJ/T 380, Technical specification for steel plate shear walls, 2015 (in Chinese)."
[52] S. Sabouri-Ghomi, C. E. Ventura, and M. H. Kharrazi, "Shear analysis and design of ductile steel plate walls," *Journal of Structural Engineering*, vol. 131, no. 6, pp. 878-889, 2005.
[53] A. Committee, "Seismic provisions for structural steel buildings (AISC 341-10)," *American Institute of Steel Construction, Chicago-Illinois*, 2010.
[54] L.-H. Han, "Flexural behaviour of concrete-filled steel tubes," *Journal of Constructional Steel Research*, vol. 60, no. 2, pp. 313-337, 2004.